
Article:
Roberts, MJ, Everson, RC, Domazetis, G et al. (6 more authors) (2015) Density functional theory molecular modelling and experimental particle kinetics for CO2-char gasification. Carbon, 93. pp. 295-314. ISSN 0008-6223

https://doi.org/10.1016/j.carbon.2015.05.053

The DFT molecular modeling and experimental particle kinetics studies of CO_2-char gasification.

Mokone J. Roberts[a*], Raymond C. Everson[a], George Domazetis[b,c], Hein W.J.P. Neomagus[a], J.M. Jones[d], Cornelia G.C.E. Van Sittert[e], Gregory N. Okolo[a], Daniel Van Niekerk[f], Jonathan P. Mathews[g]

[a]Coal Research Group, School of Chemical and Minerals Engineering, North-West University, Potchefstroom Campus, Private Bag X6001, Potchefstroom, 2520. South Africa

[b]Chemistry Department, La Trobe University, Melbourne, VIC 3086, Australia

[c]Clean Coal Technology Pty. Ltd., Melbourne, Australia

[d]Doctoral Training Centre in Bioenergy, School of Chemical and Process Engineering, University of Leeds, Leeds LS2 9JT, UK

[e]Laboratory of Applied Molecular Modelling, Chemical Resource Beneficiation, North-West University, Potchefstroom 2520, South Africa

[f]Sasol Technology (Pty) Ltd, Box 1, Sasolburg 1947, South Africa

[g]John and Willie Leone Family Department of Energy and Mineral Engineering, The EMS Energy Institute, The Pennsylvania State University, University Park, PA 16802, USA

*Corresponding author: Mokone J. Roberts. Email address: mok.roberts@nwu.ac.za and mokone.roberts5@gmail.com. Tel: +27182991997 and +27123868092. Fax: +27182991535

Abstract

Experimental measurements and DFT atomistic modelling were conducted to elucidate the mechanisms for gasification chemistry of char with CO_2 gas. The molecular models used were based on experimental representations of coal chars derived from the vitrinite- and inertinite-rich South African coals at 1000 ℃. The HRTEM and XRD techniques were used to construct parallelogram-shaped PAH stacks of highest frequency in the vitrinite-rich (7x7) and intertinite-rich (11x11) char structures. Computations were executed to get the nucleophillic Fukui functions, at DFT-DNP level, to elucidate the nature and proportions of carbon active sites and quantify their reactivity. The DFT-DNP-computed reaction pathways and transition states, to obtain the energy of reaction and activation energies for the gasification reactions of CO_2 with active carbon sites were examined. These results were compared with TGA experimental results at 900-980℃. The mean nucleophillic Fukui function of the H-terminated char models and active sites located at similar edge positions

decreased with increasing size of char molecules and followed the sequence: zigzag>armchair>tip active sites. The mean DFT-DNP values for the activation energy of 233 kJ mol^{-1} at the reactive carbon edge was in agreement with the experimental 191±25 kJ mol^{-1} and 210±8 kJ mol^{-1} for the respective chars.

Nomenclature

Symbol	Definition	Units
$\bar{X}$	Arithmetic mean	-
Δ_1	Frequency of modal class minus that of previous class	-
Δ_2	Frequency of modal class minus that of following class	-
ΔE_b	Atomistic activation energy or energy barrier by generalized synchronous transit method (~E_a)	kJ mol^{-1}
ΔH	Enthalpy	kJ mol^{-1}
1-scf	Single point energy calculations (Simulations)	-
C	Number of aromatic carbons per cluster	-
c	Size of interval	-
C*	(Re)active carbon site	_
C_f	(Re)active carbon site	_
CP-MAS	Cross polarisation-magic angle spinning	-
d_{002}	Inter-layer spacing for a group of N_{ave} parallel layers	Å
DMol^3	A modelling program that uses DFT	_
E_a	Activation energy	kJ mol^{-1}
E_{reac}	Reaction energy by generalized synchronous transit method (~ΔH)	kJ mol^{-1}
$f^+(r)$	Nucleophillic Fukui function	-
$f^-(r)$	Electrophillic Fukui function	-
$f^0(r)$	Radical Fukui function	-
F_1	Function of absolute temperature	-
F_2	Function of CO_2 partial pressure, order of reaction, and lumped pre-exponential factor	-
f_a	Carbon aromaticity,	-
k'_{so}	Lumped pre-exponential factor	min^{-1} bar^{-m}
L	Lower boundary of median interval	Å
L_0	Total pore length per unit volume	m m^{-3}
L_a	Crystallite diameter	Å
M	Median	Å
N	number of data points used	-
n	Reaction order	-
P_{CO2}	Partial pressure of CO_2 gas	Pa
R_i	Initial reactivity of chars	min^{-1}
r^L	Lumped reaction rate	m s^{-1}
r_s	Reaction rate	m min^{-1}
S	Standard deviation	-
S_0	Initial surface area	m^2 m^{-3}
t	Time	s and min
T	Absolute temperature	℃ and °K
$t_{0.9}$	Time for fractional carbon conversion of 90%	min
v_{TS}	Single negative frequency from generalized synchronous transit method	cm^{-1}
X	Fractional conversion of carbon	-
SK	Skewness	-

Greek symbols

Symbol	Definition	Units
$\mathcal{E}_0$	Initial porosity of char samples	%
θ	Peak position / XRD angle of scan	radians
γ	Gamma band/peak	-
ψ	Dimensionless structural parameter for char pores	-

Abbreviations

Acronym	Definition
ALS	Advanced Laboratory Solutions
C-C	Carbon to carbon bond/site
CHPC	(National) Centre for high performance computing (Cape Town)
DFT	Density functional theory
DIIS	Direct inversion of the iterative subspace (for SCF convergence)
DNP	Double numerical polarization basis set
DTA	Differential thermal analyser
f(r)	Fukui function
$f^{+}(r)$, $f^{-}(r)$, $f^{0}(r)$	Nucleophillic, Electrophillic, radical Fukui functions
GGA	Generalized gradient approximation
HOMO	Highest Occupied Molecular Orbital
HPC	High performance computing (NWU)
HRTEM	High resolution transmission electron microscopy
LAMM	Laboratory of applied molecular modelling (NWU)
LUMO	Lowest Unoccupied Molecular Orbital
LST	Linear synchronous transit (method to search for TS)
MEP	Minimum energy pathway
NMR	Solid state nuclear magnetic resonance spectroscopy
NWU	North-West University
PAH	Polyaromatic hydrocarbons
PES	Potential energy surface
QOF	quality of fit
QST	Quadratic synchronous transit (method to search for TS)
RMS	Root-mean-square for convergence
RPM	Random pore model
SCF	Self-consistent forcefield
SEM	Scanning electron microscopy
TGA	Thermogravimetric analyser
TPD	Temperature-programmed desorption
TS	Transition state
XRD	X-ray diffraction

1. Introduction

Economic and environmental constraints necessitate research into higher efficiency coal utilisation, to develop advanced technologies with reduced greenhouse gas emissions. A study of coal gasification is part of this effort. Coal gasification is a complex process that involves reactions with O_2, H_2O, H_2 and CO_2, either as a single component reactant or a mixture of two or more of the gaseous reagents. Gasification reactions have been studied using a variety of experimental and theoretical techniques [1-14] over a lengthy period [15] because of their importance to a variety of applications.

Various aspects of coal gasification by CO_2 and its application to oxy-combustion has been reviewed by Irfan et al. [9], where the dependence on coal rank, pressure, temperature, gas composition, catalyst and the minerals present inside the coal, heating rate, particle size, and diverse reactor types was established. A large volume of literature has been devoted to mechanisms for the gasification reactions of carbon by oxygen-containing gases through experimental methods that included thermogravimetric techniques, evolved gas analysis, TPD, transient kinetics, as well as other characterisation techniques such as SEM, HRTEM and XRD [6, 16-19]. This work highlighted the effect of structural properties of chars in gasification reaction mechanism and continues to elucidate the intricacies of coal gasification. Quantum mechanics modelling studies have contributed to the evaluation of medium- to high-temperature interactions between carbonaceous material and oxygen carrying gases [20-28]. High-level molecular modelling techniques used to carry out comprehensive study of coal gasification reactions are often confronted with the complex nature of the large coal and char structures, which present challenging computational requirements. A better understanding of associated atomistic reaction mechanism may facilitate improvements in the evaluation of coal char gasification kinetics, including rates and efficiencies. Rates of gasification of porous carbons are affected by parameters such as active site concentration, accessibility of the reactant gas into the internal area of the char, and presence of active catalysts that mediate in reactions with gasification agents [24, 29-37].

While molecular modelling studies have been conducted into the reactivity of oxygen, steam and CO_2 with carbonaceous material [28, 38-43], the models used were not directly derived models from high rank coal. Other work has focused on the chemisorption of oxygen-carrying gases on carbonaceous surfaces [28, 39, 40, 42], while Montoya et al. used ab initio

techniques to model the kinetics of elementary reaction in carbonaceous material [38]. Radovic et al. compared different chars in the C-CO_2 reaction using DFT and found that char gasification may be a structure-sensitive reaction [44]. DFT was used to model the active carbon sites responsible for reaction with the oxygen-carrying gases and to highlight a dissociative-chemisorption reaction of CO_2 on active carbon sites [28, 30, 43].

The present investigation deals with reaction mechanisms between the CO_2 and coal chars, using DFT molecular modelling, and experimental techniques, to evaluate the chemistry at active sites in char, and to examine how modeling results using a simple molecular model compare with experimental data from slow-heated, or hard-cooked, and de-ashed chars derived from the South African inertinite- and vitrinite-rich coals.

2. Chars and methodology

Experimental work relevant to molecular models is based on: (i) the characterization of two de-ashed chars, and (ii) constructing a molecular model based on HRTEM data from these chars [45].

2.1 Char molecular models

The chars were prepared by heating inertinite- and vitrinite-rich South African Gondwana coals of the Permian Age to 1000 ℃ in a packed bed reactor, at 20 ℃ min^{-1}, in Nitrogen, maintaining this temperature for 60 min, and then cooling [45]. The Nitrogen flow rate was 1.5 dm^3 min^{-1} to ensure a rapid escape of volatile matter in an inert atmosphere, and averting secondary reactions [45-47]. The chars were de-ashed by HCl-HF treatments [48-52] and characterized using petrographic, HRTEM, NMR and XRD techniques, similar to Roberts et al. [45].

The char models used for modelling studies were based on the HRTEM results shown in Figure 1; the method of parallelogram catenations by Mathews et al. was used to calculate size distribution of aromatic carbon sheets [53, 54]. This technique involves intensive image processing of the photo-micrographs (Figure 1(a)) to extract skeletonised lattice fringes (Figure 1(b)) following an approach of Sharma et al. [55]. A relationship between these

lattice fringes and aromatic carbon sheets of coals (Figure 1(c)) was used to calculate the distribution of the parallelogram-shaped aromatic molecules of the chars (Figure 1(d)) [53]. The detailed table of results is presented in Roberts et al. [45]. The modal values, calculated from Equation (1), of the grouped aromatic fringe length distributions for the inertinite- and vitrinite-rich chars were 36.8 and 21.0Å, respectively. Both distributions were positively skewed at 2.4 and 3.1, respectively, according to Pearson's second coefficient of skewness [56], Equation (2), where the vitrinite-rich char was more skewed to smaller values. The modal values correspond with the 11 by 11 and 7 by 7 carbon rings of the respective chars, based on the assumption that the fringes are as deep as they are wide, of parallel catenation, and that the number of carbon atoms, and thus number of rings, can be determined as the mean from the longest and shortest possible orientations [53, 57]. It also assumes no curvature or defects [57, 58]. The results from XRD and HRTEM techniques showed a reasonable agreement. The HRTEM modal value for the 1000 ℃ inertinite-rich chars compares well with the crystallite diameter measured by the XRD technique, L_a (10), of 37.6Å. However, the L_a (10) of 30.7Å for the vitrinite-rich chars was higher than the corresponding modal value.

$$Mode = L + \left(\frac{\Delta_1}{\Delta_1+\Delta_2}\right)c \quad (1)$$

$$SK = \frac{3(\bar{X}-M)}{S} \quad (2)$$

2.2 DFT computational methods

The DFT computational requirements restrict the model size for tractable calculations, and the utility of a single graphene sheet to model coal char is a major concern of the present studies. The SCF convergence for the 11x11 and 7x7 char models was difficult even if conversion were accelerated by the smearing tool from the default value of 13.1 kJ mol^{-1}, with small increases up to 525.1 kJ mol^{-1}. Thermal smearing is a setting applied to the orbital occupation to improve the SCF convergence within the specified number of iterations. Consequently, it was necessary to reduce the aromatic carbon sheets of 7x7 from the vitrinite-rich char and 11x11 from the inertinite-rich char, to smaller sizes of 3x3 and 5x5, respectively, by applying a factor of approximately two. However, the authors acknowledge that if the number of electrons in two structures are different, then one cannot compare the electronic energy directly. In addition to this, the 4x4-carbon ring structure was included to

create additional data point, since it was also present in both the vitrinite- and inertinite-rich chars [45]. While this approach was taken, it was noted that the electronic states of the graphene models are greatly dependent on the model size so that the energetic values such as adsorption energies and activation energies are affected, as pointed out by Pham and Truong [59]. Therefore, this investigation recognizes the sensitivity of the computed results to the simple molecular models, as the experimental data is derived from coal derived chars, which are expected to contain a variety of carbon active sites (and correspondingly variety of possible electronic configurations).

The edge carbons of the aromatic carbon sheets from the HRTEM were terminated with hydrogen to give polyaromatic hydrocarbon (PAHs) char models, following Radovic and Bockrath assertions that structures with entirely free edge carbons were unlikely, but likely with hydrogen termination. However, hydrogen termination may be appropriate for lower temperature chars, but less so for chars at high temperatures [60]. Under gasification conditions at high temperatures, thermal decomposition and abstraction of edge hydrogen would be anticipated [41]. It is also probable that the coal-derived chars contain numerous activated C* sites, so that a simple graphene molecule containing one C* active site represents an unlikely model. This difficulty cannot be overcome with the limitations of current computational resources, and in this work, the graphene model is used with a number of active sites derived through the loss of edge hydrogen groups; we acknowledge the difficulties inherent in this approach and emphasize the limitations in our current molecular modeling capabilities. It is also understood that gasification includes other reactants (H_2, H_2O, CO_2 and O_2), but the current modelling deals solely with reactions involving CO_2 [41, 61, 62]. It is also necessary to restrict the present modeling to reactions involving CO_2, as modeling gasification involving a number of gases is outside our current capabilities. We utilize simple systems to provide insights on likely mechanisms in complicated, practical systems, with the additional input from experimental data, which enables an assessment of the computational results against experimental ones.

The modeling study discussed in this paper commences with the loss of H to form a reactive carbon edge or free active sites, followed by chemisorption of CO_2 and subsequent formation of CO. The modelling results are compared with the experimental to assert the viability of the proposed mechanisms for CO_2 gasification of char derived from bituminous coal medium C rank.

Molecular models have been proposed to simulate structures with various types of active sites, e.g. the basal plane, armchair, zigzag and tip [24, 28, 39-42, 60, 63, 64]. Solid-state ^{13}C nuclear magnetic resonance (NMR) techniques [65, 66], have shown that coal chars commonly consist of structures of aromatic stack/clusters of 12-25 aromatic carbon atoms (3-7 benzene rings) [38, 67]. NMR analysis of 1000 ℃ however, encounters line broadening which prevents calculation of structural parameters, and thus it cannot predict the aromatic carbon cluster size under these conditions [65]. Line broadening is attributed to aromatic free radicals that begin to change the relaxation behaviour of the aromatic carbons [68]. Most characterization results have indicated that the 1000 ℃ inertinite- and vitrinite-rich coal chars behaved in a similar way, except for the aromatic fringes and L_a (10) values from the HRTEM and XRD techniques, respectively. These considerations provide a rational for using the reduced modal PAH structures of 7x7 and 11x11 PAHs as models of the respective inertinite- and vitrinite-rich chars, for DFT computations.

2.2.1 DFT reactivity modelling procedures with the Fukui function

The DFT geometry optimization of our char models were performed using with the DMol^3 method in the Accelrys Material Studio® software (version 6.0) using the Laboratory of Applied Molecular Modelling (LAMM) high performance computing (HPC) resources of the North-West University in Potchefstroom and the National Centre for HPC in Cape Town, South Africa. The DMol^3 calculations give accurate self-consistent field (SCF) densities as discussed in [69] and numerically localized basis sets yields improved enthalpies for the formation of H, N, O, F, Cl, C, Si, S atoms. The exchange-correlation potential of generalized gradient approximation (GGA) functional of Perdew and Wang (PW91) was used [70, 71]. Delley found that the DFT performance in predicting molecular enthalpies of formation of metallic solids was significantly improved for the Perdew–Burke–Ernzerhof (PBE) functional in comparison with PW91 [69]. However, several publications on investigations similar to the current (search for transition state) used PW91 functional [72-75]. This package provides electronic wave functions which are expanded in a double numerical coupled with polarization basis set (DNP) truncated at a real space cut-off of 4.4Å. The DNP is comparable to Gaussian 6-31G** basis set used for molecular and solids calculations, but the DNP is reported to be more accurate than the 6-31G** set of the same size [76, 77]. All the

calculations were spin-unrestricted. The default convergence tolerances used for the energy, force, and displacement were of 0.1 kJ mol^{-1} (2 x 10^{-5} Ha), 10.5 kJ $mol^{-1}Å^{-1}$ (0.004 Ha $Å^{-1}$) and 5 x 10^{-4} nm (0.005Å), respectively. The SCF was left on fermi, which required up to eight times the maximum number of iterations (1000) for convergence. This was coupled with the direct inversion of the iterative subspace (DIIS) technique developed by Pulay [78].

The 1-scf energy calculations were performed with the Accelrys Material Studio® software package on geometry optimised structures to determine the reactivity indicator using the Fukui function. The Fukui function, f(r), is among the most commonly used reactivity indicators [79, 80]. The Fukui function is usually given as the change in the density function of the molecule as a consequence of changing the number of electrons in the molecule [80] and allows a chemical reaction to be understood in terms of the highest occupied molecular orbitals and lowest unocupied molecular orbitals [81]. The function $f^{+}(r)$ is a measure of reactivity toward a donor reagent (nucleophillic attack), $f^{-}(r)$ values measure reactivity toward an acceptor reagent (electrophilic attack) and an average value of both may be taken as a measure of reactivity toward a radical $f^{0}(r)$ [82]. Parr and Yang showed that sites in chemical species with the largest f(r) value are those with highest reactivity and are the preferred reaction site(s) [83-85]. Research has emphasised that hardness-softness f(r) derived from the DFT are powerful tools to predict active sites of a molecule [84, 86, 87]. The f(r) defines the reactivity of an atom in a molecule and, together with local softness, are suitable to describe reactivity of different substrates [88], including symmetrical char structures. Here, the objective is to predict reactivity of all H-terminated and selected, free edge carbon atoms from simplied coal char structures/molecules with oxygen atoms from CO_2 gas molecules, which is anticipated as the first chemical interaction step associated with the CO_2-char gasification reaction mechanism. The O from the CO_2 atom participates as electron donor to chemisorb to the free edge carbon atom, thus making the nucleophilic Fukui function, $f^{+}(r)$, the preferred index to predict reactivity. The $f^{+}(r)$-based reactivity analyses were first conducted on H-terminated edge carbon sites to gather the rationale for the the free active sites (reactive edge) to be used in the CO_2-char gasification reaction mechanism. The energetics of the loss of H were examined using the TS theory approaches available in the Accelrys Material Studio® software package. The relative accuracy of these computations were inevitably restricted by the very large compuational resources required for these calculations.

2.2.2 DFT modelling of char-CO_2 gasification reaction mechanism

A general mechanism of the reaction of CO_2 gas with solid carbon surfaces is given by Equations (3)-(6) [89]. Initially, the CO_2 gas molecule is chemisorbed on the active site C_f on the char surface [28, 30, 64, 90, 91].

$$C_f + CO_2 \rightarrow C_f(CO_2) \quad (3)$$

This is followed by dissociation of the adsorbed CO_2 to form CO according to Equation (4), and an oxygen surface complex (quinone) on the char surface, $C_f(O)$, which is [28, 91, 92].

$$C_f(CO_2) \rightarrow C_f(O) + CO \quad (4)$$

The subsequent formation of an additional CO molecule results from the O-complex forming CO, (gasifying) with the solid carbon on the edge of the char surface, and escaping as a CO gas molecule as in Equation (5) [9, 20, 92]. Montoya et al. has shown that the six-member ring containing the O-complex ($C_f(O)$) undergoes bond weakening and breaking to form the CO gas molecule. This ring may collapse to form a five-member ring with loss of CO, or the loss of CO may accompany the formation of a defect which would act as another active carbon site, to continue the process of CO_2 gasification [38].

$$C_f(O) \rightarrow CO \quad (5)$$

Equations (3)-(5) summarise the Boudouard reaction shown in Equation (6) [31, 93]; the mechanisms however include intermediate reactions associated with the bond weakening, breaking, and re-arrangements.

$$C + CO_2 \rightarrow 2CO \quad (6)$$

The Boudouard reaction [31, 93] mechanism was examined by application of TS theory, based on a generalized synchronous transit scheme, which E_{reac} and ΔE_b [94-96] from DFT modelling of the char-CO_2 gasification reaction using the 3x3 model. Transition state theory enables consideration of transition rates in diffusion reactions and also energy profiles between reactants and products, as discussed in [73, 97-99]; the TS for a reaction is the

geometry corresponding to the highest energy along the MEP, which gives the activation energy. In the context of reaction rates, the reactant(s) and product(s) have an initial and a final state, both of which are local minima on the PES scan accurately locating the transition state.

The TS were searched by LST/QST methods [94-96, 100]. Usually after the second QST optimization the CG refinement finds the transition state. However, in molecular systems such as the ones used here, refinement of TS geometries would require unrealistically lengthy computations, especially when the system has two or more imaginary frequencies. Consequently these computations were restrained to the location of likely TS within the context of the proposed mechanisms. A number of calculations on the TS showed that there was only one imaginary frequency, which allowed for the refinement of the TS energy using a TS Optimisation Task. The major thrust of this work relies on DFT results of reaction energies for each reaction site and energy barriers, because these results enable a direct comparison between modelling and measured data. The energetics were determined for the char-CO_2 interactions for the C-H bond breakdown, CO_2 chemisorption, CO formation through CO_2 dissociation and C-C decomposition reactions.

2.3 Experimentation: Char-CO_2 reactivity (Particle kinetics)

The objective of the experimentation undertaken was to validate the results (activation energy) obtained from the reaction rate modelling based on the molecular structure (atomic reaction rate) with results obtained using particle reaction kinetics. For this purpose, experimentation was carried out using a thermogravimetric analyser with the random pore model reaction modelling [6, 101, 102].

2.3.1 Thermogravimetric analyser

Isothermal char-CO_2 gasification experiment was carried out on a TA instruments' SDT Q600 TGA supplied by ALS, South Africa, using de-ashed chars derived from inertinite-rich and vitrinite-rich South African coals. The SDT Q600 TGA can work within the temperature control range of ambient +5 to 1500 ℃, with a platinum-rhodium Type R thermocouple; with a temperature accuracy, precision and DTA sensitivity of ± 1 ℃, ± 0.5 ℃ and 0.001 ℃

respectively. The TGA uses an alumina horizontal beam null balance with a weight sensitivity of 0.1 μg, weight accuracy of ±0.1% and a repeatability of 99.9%. The controlled temperature zone of the furnace is 50 mm. Gas flow through the TGA furnace is uni-directional over the horizontal balance, thus, a purge gas counter-flow is not needed during experiments. The TGA also come with two in-built mass flow controllers, which control the gas flow rates.

2.3.2 Experimental procedure

The isothermal gasification experiments were carried out with CO_2 gas at atmospheric pressure and isothermal temperatures of 900, 920, 940, 960 and 980 ℃. Sample mass of 10 ± 1 mg of -75 μm particle size was used for each of the experiments on the TGA. The sample was loaded into a 90 μL porous alumina sample holder carefully placed on the balance pan before closing the furnace. The set-up (furnace and sample) was flushed with nitrogen gas at 100 cm^3 min^{-1} for 25 min to evacuate any oxidizing species in the furnace, as well as to stabilize the balance. The sample was heated at 30 ℃ min^{-1} under the N_2 gas flow to the required temperatures. The N_2 gas was automatically turned off and the CO_2 gas entered at a flow rate of 45 cm^3 min^{-1} for the isothermal gasification experiments. Reaction times for the experiments varied from 36 to >48 hours, similar to Everson et al. [1, 6].

2.3.3 Calculation of activation energies

The intrinsic reaction rate equation based on the random pore model was evaluated according to the method proposed by Everson et al [101] involving essentially: (1) the determination of the lumped reaction rate consisting of the intrinsic reaction rate and the initial physical properties of the chars, and (2) the determination of the activation energies and pre-exponential factors using the Arrhenius equation using the lumped reaction rate determined from the experimental results.

The relevant random pore model is in Equations (7)-(13) with a brief description of the calculation procedure. The equation for the conversion of carbon, on ash free basis, involves the reaction rate and structural behaviour, as well as characterised by the lumped reaction rate and structural parameter.

$$X = 1 - \exp\left[- r^{L} t \left(1 + \frac{r^{L} t \psi}{4} \right) \right] \tag{7}$$

$$r^{L} = \frac{r_s S_o}{(1 - \varepsilon_o)} \tag{8}$$

$$r_s = k_{so} \exp\left(\frac{- E_a}{RT} \right) \cdot P_{CO_2}^{n} \tag{9}$$

$$\psi = \frac{4\pi L_o (1 - \varepsilon_o)}{S_o^2} \tag{10}$$

For the evaluation of the lumped reaction rate, the structural parameter needs to be evaluated, which can be accomplished with Equation (11) involving regression with the unknown structural parameter. This equation can be derived from Equation (7) and can be seen to be independent of temperature (reaction rate) and is a convenient method to determine the structural parameter.

$$\frac{t}{t_{0.9}} = \frac{\sqrt{1 - \psi \ln(1 - X)} - 1}{\sqrt{1 - \psi \ln(1 - 0.9)} - 1} \tag{11}$$

With a known structural parameter, the lumped reaction parameters can be calculated also by regression with the Equation (7) and the experimental results. From a knowledge of the lumped reaction rate as a function of temperature, the Arrhenius equation parameters can be calculated using the logarithmic form of a combination of Equations (8) and (9), to yield Equations (12) and (13) [6, 101].

$$\ln(r^{L}) = -\frac{E_a}{RT} + n \ln(P_{CO_2}) + \ln(k_{so}^{'}) \tag{12}$$

$$\ln(r^{L}) = F_1(T) + F_2(P_{CO_2}, n, k_{so2}^{'}) \tag{13}$$

3. Results and discussion

The utility of single graphene sheets (or ribbons) as models for coal-char gasification studies presents a number of challenges. Pham and Truong have shown the size of the graphene

ribbon increases in length and width, its orbital energy gap decreases, with the lowest energy gap obtained for ribbons of length >8; they also demonstrate the errors in the total energies as a function of the ribbon length at different levels of theory [59]. The present work involves the size of the graphene structure consistent with the low energy differences reported by Pham and Truong [59]. This work also uses the Fukui function as an indicator of reactivity [79, 80] for edges on the graphene structure. The standard Fukui function concept of conceptual DFT includes the contribution from HOMO and the LUMO [81], but also from other chemically relevant orbitals. While the treatment by Radovic may provide particular insights related to electronic states and spin crossover effects, some of the DFT results (e.g. suggesting exothermic chemistry for CO dissociation involving small grapheme ribbons and CO_2) appear counter intuitive [28]. Of greater concern, however, is the large difference between the molecular structure of a single graphene sheet, and that of freshly formed coal-char, which is three-dimensional and disordered to varying degrees, and may form a variety of active sites during pyrolysis of coal as it undergoes heating in a gasifier. These considerations have caused the present investigation to emphasise the endothermic aspects of char gasification by CO_2, and to seek energy of reaction from the model for comparison with experimental data. Detailed studies of electronic states would need additional work with a larger char model, requiring considerably greater computational resources that are currently available and would be reported in a separate paper.

Fukui function as a reactivity indicator, allowed for the modelling sequence that commences with loss of hydrogen to form active C* sites, followed by chemisorption of CO_2, gas molecule and the energies obtained for thermal dissociation of CO_2 to form the first CO gas molecule, and thermal breakdown to yield the second CO gas molecule. Clearly, this sequence is a simplification of the actual gasification process observed in practice. The mechanism, however, is elucidated using both computed values of ΔE_b and E_{reac} and their comparison with experimental data.

3.1 DFT reactivity modelling and the Fukui function

Substantial research have found that the chemical interactions between carbon molecules and reactant gases take place at the edge active carbon atoms for coal based char models and also for non-coal char models [3, 28, 39, 43, 60, 64, 103-105], and Zhang et al. found that the

carbons in the basal plane of large, fused-ring aromatic domains of chars, were inert [106]. Figure 1 shows results from the HRTEM technique, which were used to derive the char models used here [45].

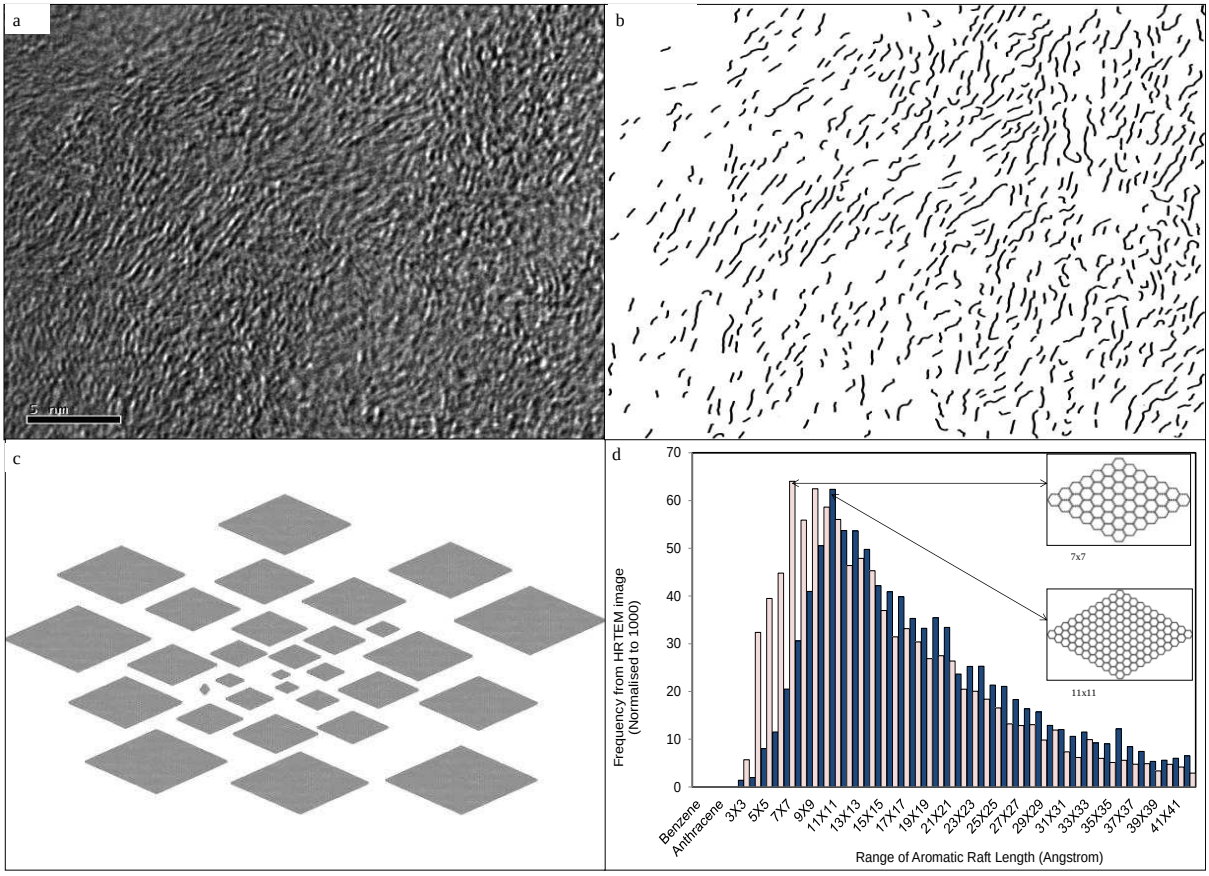

Fig 1. HRTEM results. Microphotograph for the inertinite-rich chars ((a), top left), with scale bar = 5 nm. Lattice after image processing ((b), top right). Parallelogram catenations ((c), bottom left). Distributions of aromatic raft lengths ((d), bottom right), where, dark and light bars = inertinite- and vitrinite-rich chars, respectively.

The char-CO_2 reaction mechanism commenced with reactivity analysis of the H-terminated edge carbon atoms using the $f^+(r)$ values. Results from here were used to rationalise the selection of free active edge carbon atoms, which involved the loss of H from C-H edges, using the transition state theory. The definition, position and numbering of H-terminated C active sites are presented in Table 1 accompanied by Figure 2. The $f^+(r)$ results are presentated in Table 2(a)-(c) at an accuracy of ±0.001. The $f^+(r)$ is a dimensionless reactivity index.

Table 1. Definition of H-terminated edge carbon sites, including position and quantity.

Edge C name	Symbol	3x3	4x4	5x5
Tip	C_t	C1, C29	C1, 47	C1, C69
Zigzag, proximate to tip	C_z	C2, C6, C28, C30	C2, C6, C46, C48	C2, C6, C68, C70
Zigzag, remote from tip and armchair	C_{zi}	C7, C13, C23, C27	C7, C14, C21, C22, C31, C40, C43, C45	C7, C14, C15, C25, C26, C33, C49, C54, C55, C62, C65, C66
Armchair	C_{r1}, C_{r2}	C14, C15, C20, C21	C15, C16, C28, C29	C21, C22, C34, C35

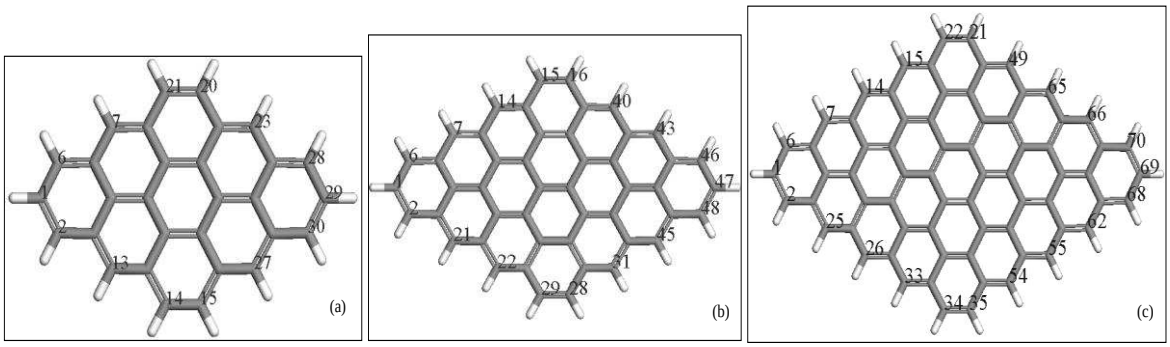

Fig 2. The PAH char models used to determine the nucleophillic Fukui values of the edge carbon sites, where (a), (b) and (c) = 3x3, 4x4 and 5x5 structures, respectively.

The results indicate that reactivity of H-terminated char models and active sites located at similar edge positions decreases with increasing size. In addition to this, the reactivity analysis of the respective char models show that the $f^+(r)$ of all zigzag (C_z) carbon sites adjascent to the tip was similar, but decreased with remoteness of intermediate zigzag sites (C_{zi}) from the tip. The reactivity values follow the sequence: zigzag > armchair > tip.

The Fukui function values on the H-terminated edge carbons are taken as indicative of the sites that would form C* active sites (reactive edge) after loss of H. This shows the reactivity of sites located at similar edge positions of the respective 3x3, 4x4 and 5x5 PAH char models was similar. This outcome was observed even if the "use symmetry" option of the program were not utilised during computations.

Table 2. Reactivity of 3x3 ((a), left-hand side), 4x4 ((b), middle) and 5x5 ((b), right-hand side) coal char models from $f^+(r)$.

(a) 3x3 PAH			
Edge site	$f^+(r)$ Milliken	Reactivity level*	Edge type
C1	0.004	4	C_t
C2	0.039	1	C_z
C6	0.039	1	C_z
C7	0.033	2	C_{zi}
C13	0.033	2	C_{zi}
C14	0.014	3	C_r
C15	0.014	3	C_r
C20	0.014	3	C_r
C21	0.014	3	C_r
C23	0.033	2	C_{zi}
C27	0.033	2	C_{zi}
C28	0.039	1	C_z
C29	0.004	4	C_t
C30	0.039	1	C_z
Mean	0.025		

(b) 4x4 PAH			
Edge site	$f^+(r)$ Milliken	Reactivity level*	Edge type
C1	0.003	5	C_t
C2	0.033	1	C_z
C6	0.033	1	C_z
C7	0.028	2	C_{zi}
C14	0.016	3	C_{zi}
C15	0.008	4	C_r
C16	0.007	4	C_r
C21	0.028	2	C_{zi}
C22	0.016	3	C_{zi}
C28	0.007	4	C_r
C29	0.008	4	C_r
C31	0.016	3	C_{zi}
C40	0.016	3	C_{zi}
C43	0.028	2	C_{zi}
C45	0.028	2	C_{zi}
C46	0.032	1	C_z
C47	0.003	5	C_t
C48	0.032	1	C_z
Mean	0.019		

(c) 5x5 PAH			
Edge site	$f^+(r)$ Milliken	Reactivity level*	Edge type
C1	0.003	6	C_t
C2	0.026	1	C_z
C6	0.026	1	C_z
C7	0.024	2	C_{zi}
C14	0.017	3	C_{zi}
C15	0.011	4	C_{zi}
C21	0.005	5	C_r
C22	0.006	5	C_r
C25	0.023	2	C_{zi}
C26	0.017	3	C_{zi}
C33	0.010	4	C_{zi}
C34	0.005	5	C_r
C35	0.006	5	C_r
C49	0.010	4	C_{zi}
C54	0.010	4	C_{zi}
C55	0.017	3	C_{zi}
C62	0.023	2	C_{zi}
C65	0.017	3	C_{zi}
C66	0.023	2	C_{zi}
C68	0.025	1	C_z
C69	0.003	6	C_t
C70	0.025	1	C_z
Mean	0.015		

* Largest $f^+(r)$ value = highest reactivity level [83-85].

It was postulated that during CO_2 gasification, the higher reactive sites such as C_z and C_{zi}, from the 3x3, will preferentially lose H. Anealling during pyrolysis however, may give rise to active sites of lower reactivity as the 3x3 grows to 5x5 sizes, because at high temperatures, and chemically-controlled gasification process, char undergoes thermal annealing in competition with gasification [106-108]. This causes the growth of crystallite diameter, L_a, by the coalescence of crystallites along the a-axis (e.g. from 3x3 to 5x5 aromatic fringes) [109] for both graphitisable and non-graphitisable carbons [109]. Zhang et al. studied the effects of pyrolysis intensity on the reactivity of coal char in chemically-controlled CO_2 gasification experiments and found the largest difference in coal char reactivity was observed in the initial stage of gasification, but, as the process continues, the active sites of high

activity were preferentially removed by CO_2 or annealed into less active site and the active sites with lower reactivity were left in residual coal char [106]. Suuberg also found that the inherent reactivity of the chars was attributed to the changes in the active site concentrations, which were often thermally induced [110]. Hence, under high temperature regimes and chemically-controlled gasification process, the char actually undergoes a process of thermal annealing (pyrolysis) in competition with gasification [106-108]. With the increase of carbon conversion or when the higher reactive sites in the 3x3 model are removed/annealed, the reactivity, and the number of reactive carbon sites reach similar levels and the difference in char reactivities becomes smaller [106, 110].

Consequently, the carbon edge (reactive edge) composed of reactive sites C_t, C_z, C_{zi}, C_{r1} and C_{r2} shown in Figure 5(b) was used to model CO_2-char gasification reactivity and to examine relative reactivities at each site.

3.2 DFT modelling for char-CO_2 gasification reaction mechanism

The utility of single graphene sheets (or ribbons) as models for coal-char gasification studies presents a number of challenges. Pham and Truong have shown the size of the graphene ribbon increases in length and width, its orbital energy gap decreases, with the lowest energy gap obtained for ribbons of length >8; they also demonstrate the errors in the total energies as a function of the ribbon length at different levels of theory [59]. The size of the graphene structure in the current investigation is consistent with the low energy differences reported by Pham and Truong [59]. The Fukui function as an indicator of reactivity for edges on the graphene structure is also used. The model has arbitrarily been used with a number of C* (H free) sites, in an effort to illustrate different reactivities even after H loss (as may be anticipated in freshly formed coal char). Detailed studies of electronic states would require additional work with a larger char model, requiring considerably greater computational resources than are currently available.

3.2.1 The loss of H to form an active site

Char models have generally used selected active sites for DFT studies on the interactions of carbonaceous surfaces and gaseous reactants, with the remaining edge carbons capped with

hydrogen atoms [20, 24, 27, 28, 39, 111]. Radovic detailed the challenges associated with the loss of hydrogen from the C-H edge carbons to form the active sites [28], while Domazetis et al., used semi-empirical modelling techniques to decribe H abstraction [33]. Radovic has proposed isolated carbene-type zigzag carbon atom and a carbyne-type armchair pair of carbon atoms [43]. While the necessity of using small molecular models may be acceptable, together with the suitability of such sites for these models, the question is how similar are these to mechanisms operating during char formation as coal particles are heated to elevated temperatures. Obviously further work is required using larger molecuar models that closer reflect the properties of coal-derived chars and this requires greater computational resources than currently available. Char formation from the coals used in the present studies has been discussed elsewhere [45]. The current investigation, because of the limitations discussed, commences by examining H loss from well-known benzene molecules and progresses to larger (3x3) char molecules. The loss of H was at the following sites: C_t, C_z, C_{zi}, C_{r1} and C_{r2}. From Table 2, the intial reactions are likely to be at the C_z and C_{zi} sites.

The C-H bond breakdown for the molecule benzene molecule, as shown in Figures 3(a)-(d), was evaluated to obtain the activation energy (energy barrier), ΔE_b and reaction energies (bond dissociation energies), E_{reac} for this simple system, defined by Equation (14) and (15) respectively.

$$\Delta E_b = Energy\ of\ the\ stransition\ state - Energy\ of\ the\ reactant \quad (14)$$

$$E_{reac} = Energy\ of\ products - Energy\ of\ reactants \quad (15)$$

Figure 3 shows the structures examined for H-loss from para-, meta-, and ortho-carbons, and the results in Table 3 show ΔE_b values of 484, 452 and 485 kJ mol^{-1}, respectively.

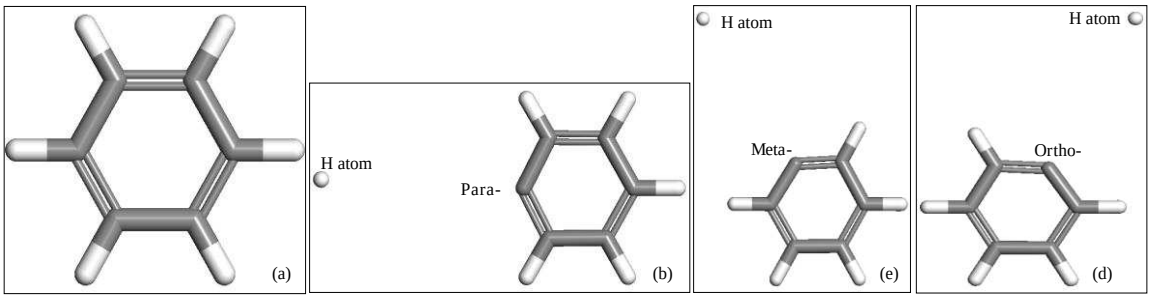

Fig 3. Geometry optimized structures for H-loss from (a) benzene molecule at (b) para-, (c) meta- and (d) ortho-carbon sites.

The mean ΔE_b value of approximately 474 kJ mol^{-1} (113 kcal mol^{-1}) for a free C-edge in benzene and E_{reac} (comparable to ΔH) for the reaction in Equation (16) [112], of 440.7, 440.4 and 443.1 kJ mol^{-1} respectively, was obtained.

$$C_6H_6 \rightleftarrows C_6H_5 + H \quad (16)$$

The values compare well with the published value of 464.0 ± 8.4 kJ mol^{-1} (110.9 ± 2.0 kcal mol^{-1}) [113, 114]. These DFT-DNP procedures, used to examine loss of H in the 3x3 PAH char model shown in Figure 4(a)-(f) at C_t-, C_z-, C_{zi}- C_{r1}, and C_{r2}-carbons, to form free active carbon edge (shown in Figure 5b), provided ΔE_b values of 489.3, 494.2, 465.9, 455.7 and 459.1 kJ mol^{-1} (Table 3). The average energy barrier ΔE_b and E_{reac} (similar to ΔH) values were repectively 472 and 446 kJ mol^{-1}, for the char structure shown in Figure 5(b). The mean value for the loss of H to form an active carbon site (reactive edge) is similar to that obtained for benzene, and similar to values for smaller and larger PAHs discussed in [113, 114]. These results illustate that the formation of active sites by loss of H from edges incurrs a high ΔE_b value.

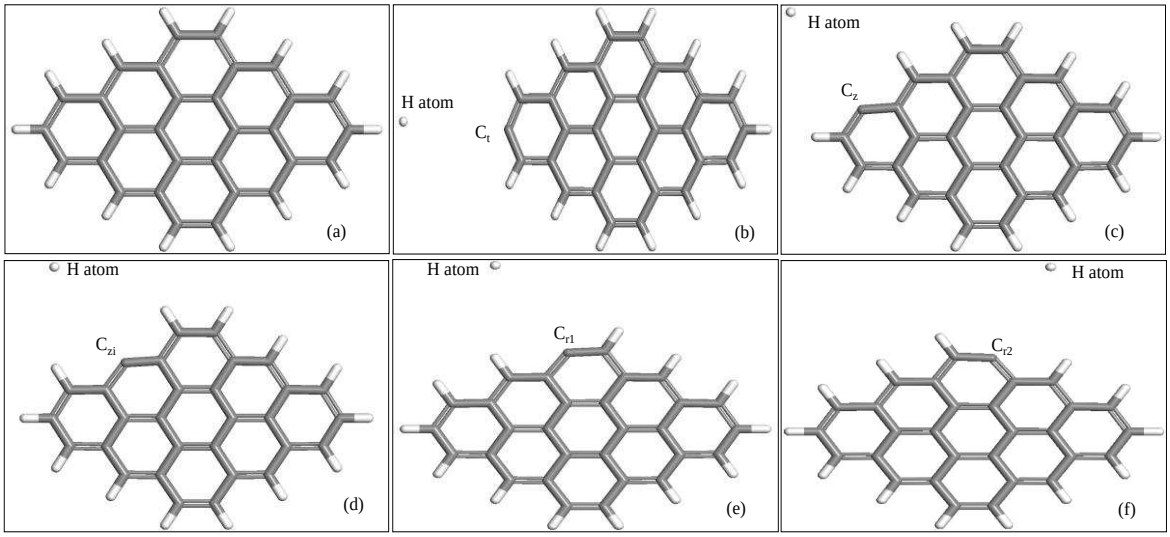

Fig 4. Geometry optimised structures for H-loss from (a) 3x3 char structure at (b)-(f) = C_t-, C_z-, C_{zi}-, C_{r1} and C_{r2}-carbons, respectively.

Table 3. Calculated ΔE_b and E_{reac} values for the loss of H from the benzene and 3x3 char structures.

Edge C positions for H-loss		ΔE_b (kJ mol^{-1})	E_{reac} (kJ mol^{-1})
Benzene molecule			
Para-		484.8	440.6
meta-		452.2	440.4
ortho-		484.4	443.1
	Average	473.8	441.4
3x3 PAH char model			
C_t		489.3	440.6
C_z		494.2	445.6
C_{zi}		464.9	448.6
C_{r1}		454.7	452.6
C_{r2}		459.1	443.0
	Average	472.5	446.1

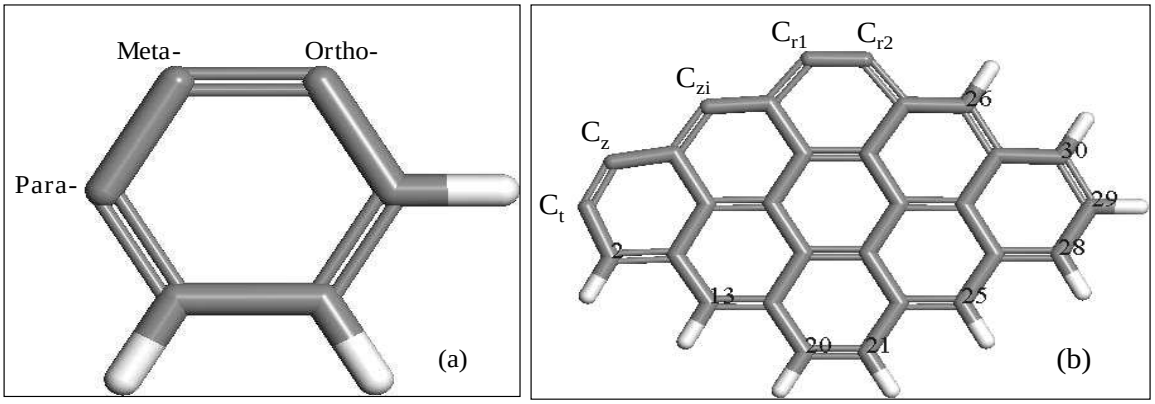

Fig 5. Structures with free edge carbon sites, where (a) = Benzene (left-hand side) and (b) = 3x3 char (right-hand side).

It is reasonable to infer from this that data on electronic states and resulting variations in computed energy values for these small molecules, but question a direct relevance to mechanisms involving coal derived char, since changes in the size of the molecular model and number of active sites, would lead to changes in electronic states. For example, it may be speculated that stacking of sheets, as found in graphite, may impact on the gammaa π delocalised electrons, and active sites located above and below edges may also impact on the electronic states and configurations of chemisorbed CO_2. Informed comment on these matters

may be enabled by computations allowing the use of large-scale char molecular models. The current work demonstrates the changes in relative reactivity for various C* actives sites, and their utility and limitations of DFT computations inherent when using small graphene molecules, to elucidate details of CO_2 coal-char gasification mechanisms.

3.2.2 CO_2 chemisorption on reactive edge

Chemisorption of CO_2 on the active sites in char has been an important area of research and has been extensively discussed [28, 30, 39, 43, 64, 115-119]. The $f^+(r)$ values were computed for the respective reactive sites to evaluate the likely locations for chemisorption, and to obtain the energy of reaction (E_{reac}) and the energy barrier (ΔE_b) at each of these sites. The DFT computations for the 5x5 char model require excessive computer resources, thus effort was restricted to the 3x3 char model. However, Montoya et al. have indicated that the heats of CO_2 chemisorption reaction remained nearly constant as the model size increased, emphasizing the chemisorption energies depend significantly on nature of the active site [39]. Table 4 shows the $f^+(r)$ values for active sites in the 3x3 char model, and the values follow the sequence: $C_{zi} > C_{r1} > C_t > C_{r2} > C_z$. The $f^+(r)$ values indicate the preferred active site is C_{zi} for CO_2 chemisorption.

Table 4. Distribution of Fukui indices on the 3x3 char model with a reactive edge.

Edge C	C_t	C_z	C_{zi}	C_{r1}	C_{r2}	C2	C13	C20	C21	C25	C26	C28	C29	C30
Mulliken $f^+(r)$	0.075	0.027	0.266	0.087	0.029	0.017	0.005	0.005	0.011	0.021	0.032	0.026	0.008	0.022

The reaction pathways for gasification of coal chars with CO_2 gas are based on the gasification reaction mechanism shown in Equations (3)-(5). Figure 6 shows the DFT-DNP geometry optimised structures for (a) the 3x3 coal char with a reactive edge, (b) the CO_2 gas molecule, (c) the 3x3-coal char structure with CO_2 gas molecule approaching at 0.5 nm distance from the C_{zi} active site and (d) the CO_2 chemisorption at site C_{zi}. Structural configurations shown in Figures 6(e)-(h) depict the CO_2 chemisorption reaction at sites C_{r1}, C_t, C_z, and C_{r2}.

The MEP includes a description of the reaction and provides the energy barrier (activation energy) and the minimum energy path between a pair of stable states [74]. A single imaginary

frequency corresponds to a point somewhere on the saddle in the potential energy scan of a given structure consistent with the TS. In geometry optimisations, there is no guarantee that the optimised structures will be at a true energy minimum. Thus, finding a thermodynamically stable structure of a molecule (without soft modes) is a major topic in structural chemistry [120]. The values for E_{reac} and ΔE_b were computed relative to the initial ground state structure of the CO_2 adsorbed on the respective active site. The results in Table 5 indicate that these are energetically favoured, with E_{reac} value consistent with CO_2 chemisorbed on the active sites, and low ΔE_b energy barriers, with a mean E_{reac} value of -11.9 kJ mol^{-1} and mean ΔE_b of 3.4 kJ mol^{-1} respectively. The lowest ΔE_b for the chemisorption of CO_2 gas molecule at C_{zi} active site is indicative of a nearly barrierless reaction and shows a good correlation with the highest $f^+(r)$ value reported in Table 4. The values are for the particular molecular model containing all of the active sites stipulated but are consistent with reports of chemisorption of CO_2 on various carbonaceous models as an exothermic process associated with low adsorption energies [28, 43, 121-123].

Table 5. Simulation energetics for CO_2-char chemisorption at the reactive edge.

Reactive edge (active C* sites)	ΔE_b (kJ mol^{-1})	E_{reac} (kJ mol^{-1})
C_{zi}	1.3	-8.4
C_{r1}‡	-	-
C_t	4.1	-19.2
C_{r2}‡	-	-
C_z	4.7	-8.2
Average reactive C edge	3.4	-11.9

‡ = Unable to find potential energy maximum for transition state.

These values are in contrast to high values reported for perfect and defective basal carbon planes by Cabrera-Sanfelix [124] and further illustrate the variations that may be obtained in these studies. The optimized configurations for CO_2 at sites -C_{zi}, -C_{r1}, -C_t, and -C_z show approximately similar bond bending behaviour of the chemisorbed CO_2 in Figures 6(d)-(f)

and (h), highlighting that the mechanism of CO_2 chemisorption obtained from the zigzag models is not significantly different from that obtained from armchair models [111, 119].

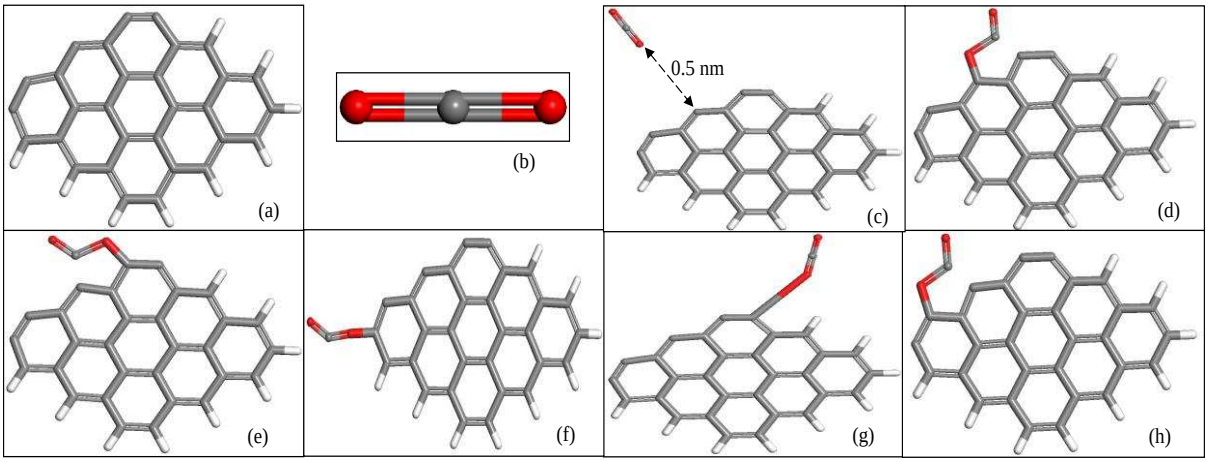

Fig 6. Various optimised structures for the CO_2 chemisorption on single active sites in the reactive C* edge. Top left is 3x3 char model with reactive edge (a). Top right is CO_2 gas model (b), (c) is the 3x3 char model with CO_2 approaching and (d)-(h) are the chemisorption structures. Red = oxygen atoms.

These E_{reac} values for the CO_2 chemisorption from the current work differ from the reported energies ranging from -355.6 to -25.1 kJ mol^{-1} at B3LYP/6-31G(d) DFT level of theory for the different char models found by Montoya et al. [39]. The difference in these computed adsorption energies is more likely due to the physical models [63]. The results indicate CO_2 chemisorption is favoured on the C_{zi} site although the numerical ΔE_b and E_{reac} values may differ for different models.

Examination of bond distances on the structures of CO_2 chemisorption at C_{zi} shown in Figure 7a indicated that, upon chemisorption, the CO_2 gas molecule assumed a zigzag shape towards C_{r1} and the O-C-O bond lengths of the CO_2 gas molecule were elongated from less than 1.2Å to 1.5Å between the chemisorbed O atom and C, and more than 1.2Å between the C and the other O atom, while the CO_2-char bond length was 1.4Å. The chemisorbed CO_2 molecule also bent towards C_{r1} at a distance of 1.5Å. Analyses of these distances with respect to formation and breakage of bonds show that C_{zi} is an ideal site for the formation of a quinone char(O)-complex and CO gas molecule from CO_2 dissociation. Similar inferences could be made with CO_2 chemisorption at C_{r1} and C_z in Figure 7(b) and (d), respectively. The ground state interactions of C_t- and C_{r2}-CO_2 respectively show weaker CO_2 chemisorption, but may be suitable for physisorption processes. The E_{reac} and ΔE_b values were not obtained for the

CO_2-C_{r1} and CO_2-C_{r2} chemisorption, because of the occurrences of multiple imaginary frequencies (soft modes) in the geometry optimised reactants and products structures, indicative of an absence of TS. Similar observations were reported by Radovic [43].

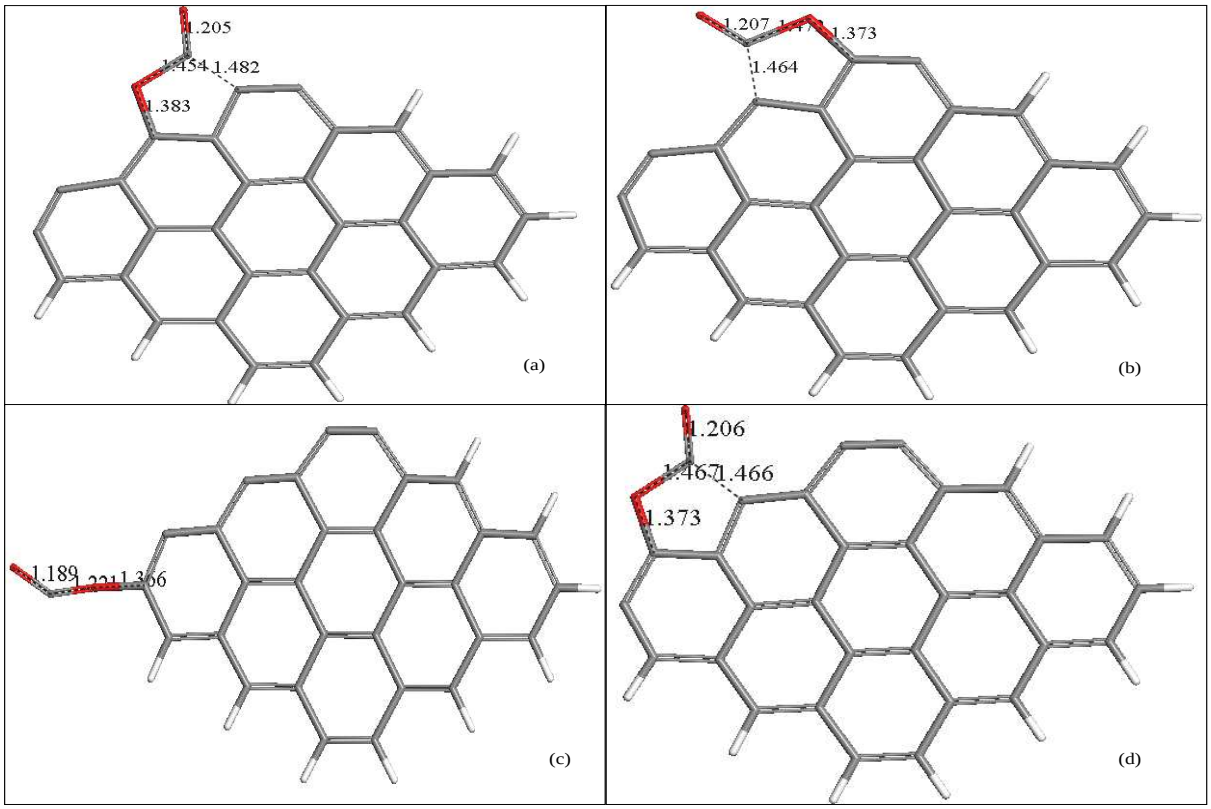

Fig 7. Bond bending and elongations of geometry optimised CO_2-C* chemisorption structures, where: red = oxygen atoms.

The change in geometry of the CO_2 chemisorbed molecule in to bent configuration, and resulting changes in the bond lengths, is indicative of additional changes in the electron configuration of the char-CO_2 molecule, and would further complicate the modeling results. Further work is required for a detailed examination of these details and to demonstrate a correlation with experimental data on char gasification.

3.2.3 The loss of first CO gas molecule through dissociation of adsorbed CO_2 molecule

In this investigation, adsorption of CO_2 on an active site is followed by the loss of CO through the dissociation of the adsorbed CO_2. This mechanism is the breakage of the char(O----CO) bond. The E_{reac} value for loss of the first CO was obtained as the difference between

the char(CO_2) structure, and the final products of char(O) plus free CO, as shown in Figure 8(a)-(b). The reaction energies for the loss of CO from the respective active sites presented in Table 6 were endothermic. The values of 576-588 kJ mol^{-1} for C_{r1}, C_t and C_{r2} compare fairly well with CO_2 dissociation energy of 526 kJ mol^{-1} in [125]. The respective values for E_{reac} and ΔE_b of 200.6 and 199.2 kJ mol^{-1} for CO_2 chemisorbed on the active site C_{zi} are lower, and nearly the same. It can be argued that these values are consistent with an endothermic thermal breakdown of the C—(CO) bond in the chemisorbed CO_2 molecule, but the range of values for all of the actives sites is unusual and may result from modelling using a number of C* actives sites.

Table 6. Computed E_{reac} (energy of reaction) and ΔE_b (energy barrier) for loss of the first CO gas molecule.

Reactive edge (active C* sites)	ΔE_b (kJ mol^{-1})	E_{reac} (kJ mol^{-1})
C_{zi}	199.2	200.6
C_{r1}	587.9	142.1
C_t	575.7	155.3
C_{r2}	575.8	132.5
C_z	185.8	168.3
Average reactive C edge	424.9	159.8

The current approach has been to obtain an average value. However it is noted that the energy barrier of 193 kJ mol^{-1} on the zigzag carbon edge, comprising C_{zi} and C_z is in good agreement with CO desorption activation energy of 130-205 kJ mol^{-1} reported by Montoya et al. [63].

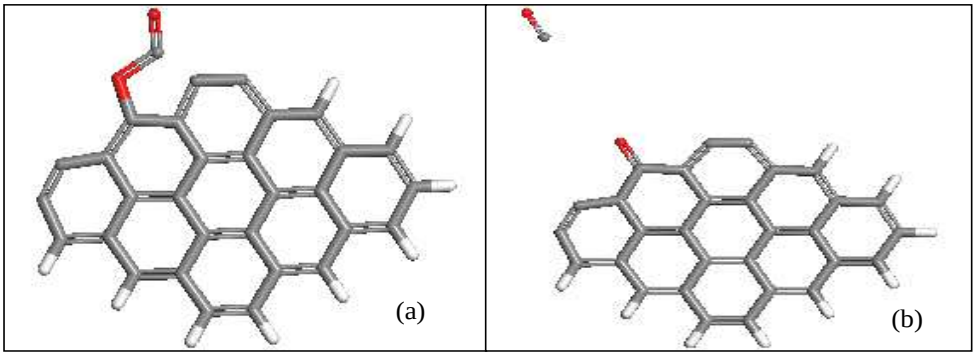

Fig 8. Ground state reactants (a), (left-hand side) and products (b), (right-hand side) structures used for the computation of CO_2 dissociation on C_{zi} active site.

When the transition state is sufficiently refined, the computational procedure will provide ν_{TS} consistent with a TS complex. In view of the modelling limitations involving char molecular systems, the available computational capabilities were used to obtain values for E_{reac} and ΔE_b only. For the current purpose, the E_{reac} value is similar to ΔH values obtained by considering the reactants and products of each step in the mechanisms considered. The most likely transition state for CO_2 dissociation involves the C_{zi} site as shown in Figure 9(a). The CO molecule is situated at a distance of 2.510Å from the quinone oxygen complex, and 2.606Å from the C* atom on the adjacent aromatic ring.

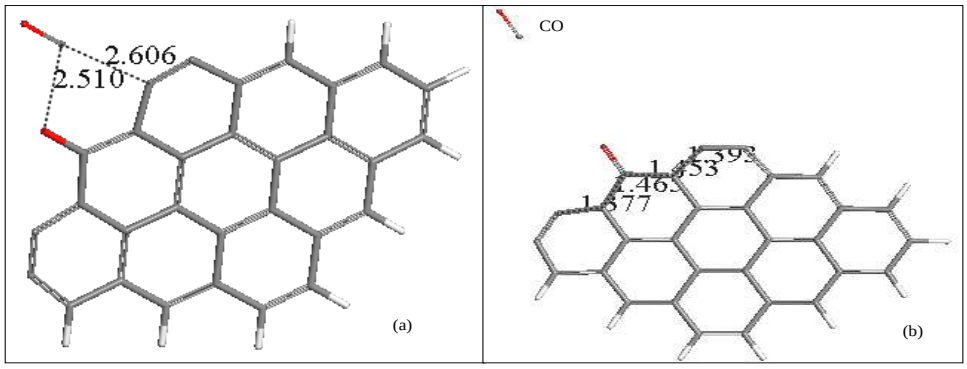

Fig 9. Transition state structure for the CO_2 dissociation at C_{zi} (a) (right-hand side). Ground state char(C=O) quinone structure and the loss of CO. Numbers = bond lengths in Å.

3.2.4 Formation of the second CO gas molecule

The chemistry considered for loss of the second CO is the thermal decomposition of the six membered carbon ring at elevated temperatures and the result is the loss of gaseous CO and formation of either a five member ring in the char substrate, or loss of CO and formation of additional active C* sites for further chemisorption of additional CO_2 molecules. The six-

member carbon ring containing the armchair and tip active sites can also form stable four- and three-membered carbon rings up on the decomposition reactios [24]. The bond lengths of the 6-member carbon ring from the geometry optimised 3x3-coal char structure are shown in Figure 9(b). Montoya et al., also investigated the loss of CO from semiquinone carbon-oxygen species in carbonaceous surfaces using ab initio/DFT (B3LYP/6-31G(d)) levels of theory [38].

Numerous computations were performed to find transition state structures for the decomposition reactions. The decomposition of the 6-member carbon ring yields a CO ($C_{zi}O$) gas molecule. However, the formation of a five-member carbon ring is considered unlikely at C_{zi} site. Instead, the formation of more active C* sites are likely [39]) and any other ring formation is unlikely because of the long C---C distance in the resulting structure, as shown in Figure 10(a).

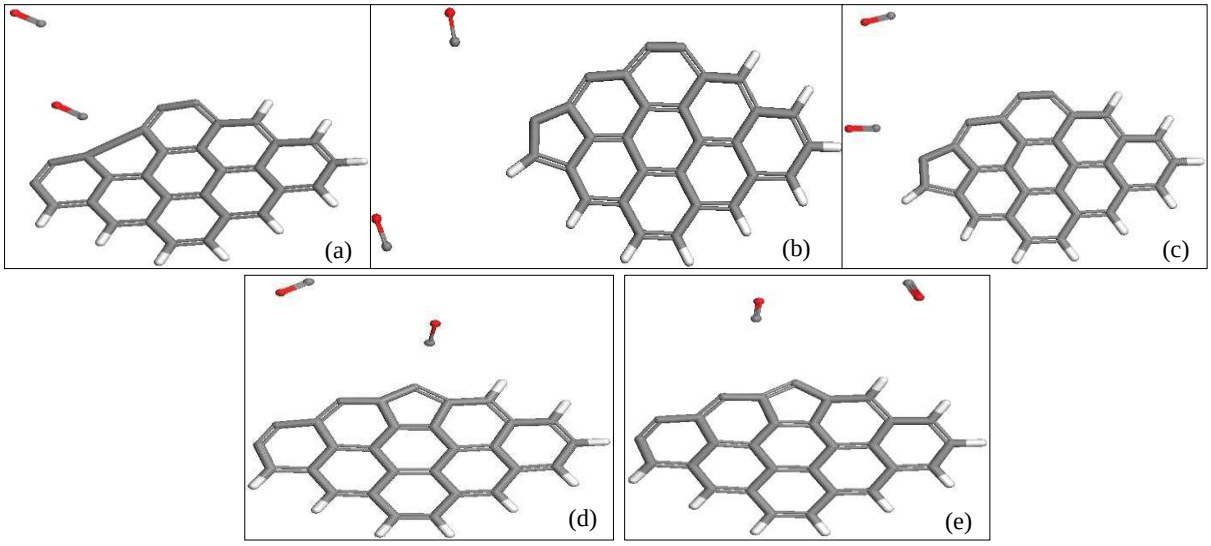

Fig 10. Transition state structures for the decomposition reactions at respective active sites (i.e. reactive edge), where, (a)-(e) = results at C_{zi}, C_t, C_z, C_{r1} and C_{r2}, respectively. Red = oxygen atoms.

The decomposition reaction energetics presented in Table 7, show both the high-energy barrier, ΔE_b, of 587.4 kJ mol^{-1} to the formation of the second CO from C_{zi} site and endothermic reaction energy E_{reac} of 187.9 kJ mol^{-1}. Loss of the second CO at C_{zi} site would require relatively higher temperatures. The high activation energy suggests that this type of semiquinone complex has an important effect on the rate-limiting step in the char gasification

mechanism and, in essence, defines gasification [119, 126]. The energy barriers ΔE_b obtained for the C_t, C_z, C_{r1} and C_{r2} sites of 68.4, 136.0, 189.5 and 183.5 kJ mol^{-1}, respectively, are substantially lower than ΔE_b for the C_{zi} site. Activation energy of approximately 360 kJ mol^{-1} was reported by of Chen and Yang [126] and approximately 340 kJ mol^{-1} was found by Sendt and Haynes [42], and values for similar models were 83-369 kJ mol^{-1} and 142-334 kJ mol^{-1} [24, 119]. The mean value for ΔE_b of 233 kJ mol^{-1} is in good agreement with the experimental value of 191 ± 25 kJ mol^{-1} and 210 ± 8 kJ mol^{-1} for the de-ashed vitrinite- and inertinite-rich chars, respectively (Section 4).

Table 7. Computed ΔE_b (energy barrier) and E_{reac} (energy of reaction) for loss of second CO gas molecule.

Reactive edge (active C* sites)	ΔE_b (kJ mol^{-1})	E_{reac} (kJ mol^{-1})
C_{zi}	587.4	187.9
C_{r1}	189.5	169.5
C_t	68.4	64.5
C_{r2}	183.5	173.5
C_z	136.0	139.9
Average reactive C edge	233.0	147.0

The TS structures for the C_t, C_z, C_{r1} and C_{r2} sites, which underwent decomposition of six-membered rings provided five-membered rings with conventional C-C bond lengths. The respective distances between the newly formed CO and the char varied (4.3Å, 2.5Å, 2.8Å and 3.8Å). These results are consistent with the ΔE_b values and indicative of the ease with which CO is lost from the various sites.

The surface transformations for the formation of both the first CO gas molecule from the CO2 dissociation reactions and the second CO from the decomposition reactions were accompanied by large endothermic energies. These endothermic reactions generally validate the bond-breaking occurrences for the yield of CO gas molecules. On the other hand, the

exothermic energies experienced by the CO_2 chemisorption reactions are generally associated with bond-forming rather than bond-breaking events. However, a mean activation energy ΔE_b for the CO_2 dissociation reactions is significantly larger than that for both the chemisorption and decomposition reactions. Inferences can be made from here that the CO_2 chemisorption was not always accompanied by dissociation and may nearly be impossible to experience dissociation at certain active sites during gasification. Zhu et al. also made similar observations [119]. There is, therefore, a likelihood that in the event that the dissociation of CO_2 did not take place, the gas remained chemisorbed on active site and simply bounced back (desorped).

The major focus of the current investigation has been to compare computer molecular modeling results obtained using a very simple molecular model with experimental results from char gasification. In this way the likely mechanisms for char gasification was identified.

4. Experimental reactivity and parameters

The conversion versus-time results for the char-CO_2 gasification reactions are shown in Figure 11, together with the predictions from the random pore model, Equation (7). The results are consistent with increasing conversion with increasing temperature and there is good agreement between the experimental results and the RPM prediction with the regressed parameters (structural parameter and lumped reaction parameters), in Equation 7. The structural parameters were found to be 2.08 and 1.08 for the inertenite- and vitrinite-rich chars, respectively, which depend on the initial properties of the chars, Equation (8). Since the limiting value for pore growth according to the random pore model is greater than a value of 2 [6, 101, 102, 106, 127] both chars can be considered to have experienced mainly pore growth and pore coalescence during the initial stage of the char-CO_2 gasification reaction. The determined values for the lumped reaction rates as a function of temperature, Figure 12, show that the vitrinite-rich char is more reactive than the inertinite-rich char. This difference is attributed to the effect of the char physical properties, Equation (8), in addition to the intrinsic reaction rate, which needs to be examined.

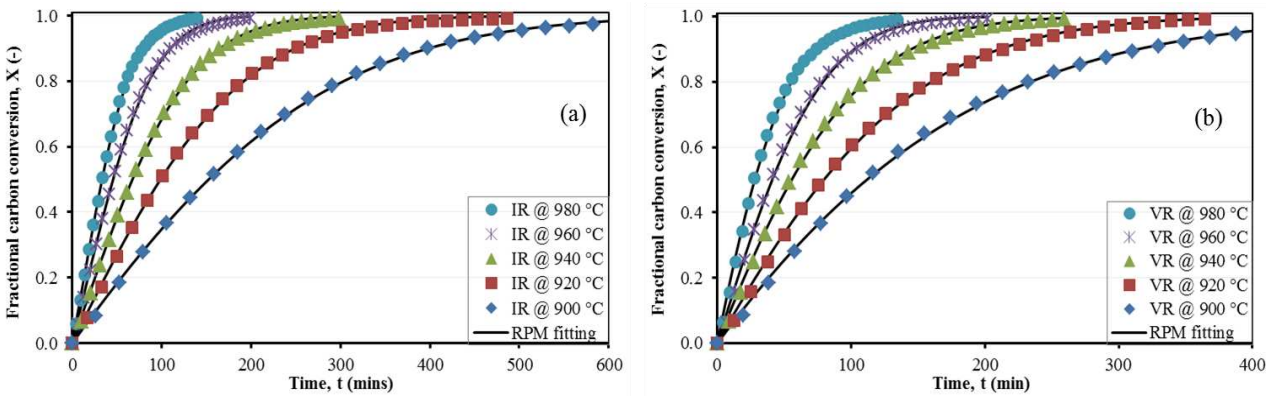

Fig 11. Conversion-time plot for inertinite- and vitrinite-rich chars, where, (a), left-hand side = inertinite-rich char and (b), right-hand side = vitrinite-rich chars.

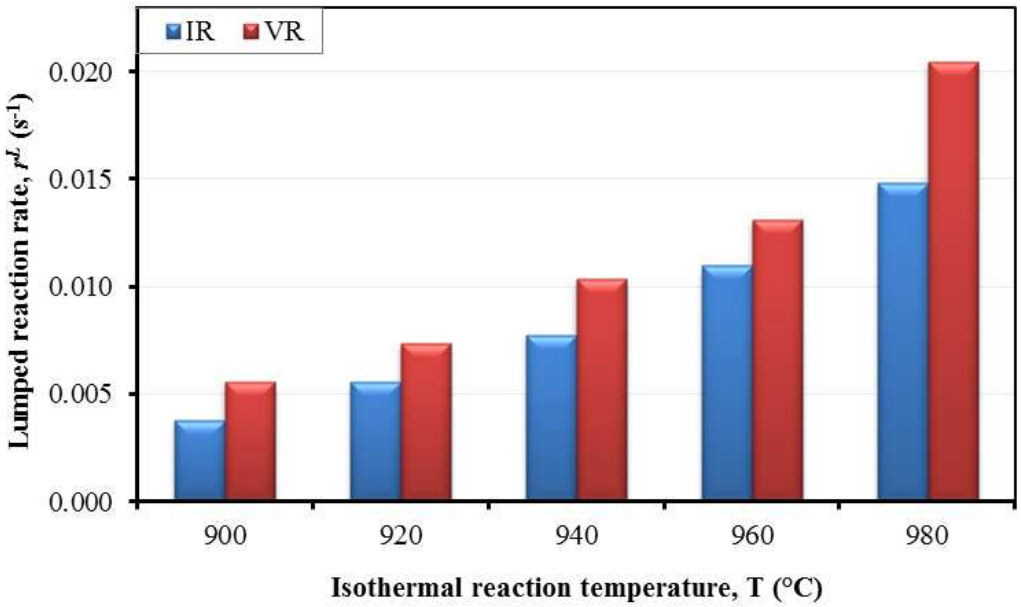

Fig 12. Influence of isothermal reaction temperatures on the lumped reaction rates of the chars.

4.1 Validation of activation energy

The experimental results consisting of the lumped reaction rates derived with the application of the random pore model, given in Figure 12, was used to validate the activation energy obtained by the DFT-DNP molecular modelling technique. The result for the two chars are shown in Figure 13. The result for the two chars are shown in Figure 13. The calculation consisted of plotting the results on a graph with semi logarithmic coordinates (ln r^L versus 1/T) and comparing the results obtained from Equation (10), using the activation energy of

233 kJ mol^{-1} reported in Section 3.2.4 together with suitable values for r^L in Equation (12), to ensure the best fit according to linear regression procedure. The agreement was found to be very good within the limits of experimental uncertainty at 95% confidence interval, as shown with the estimated activation energies in Figure 15.

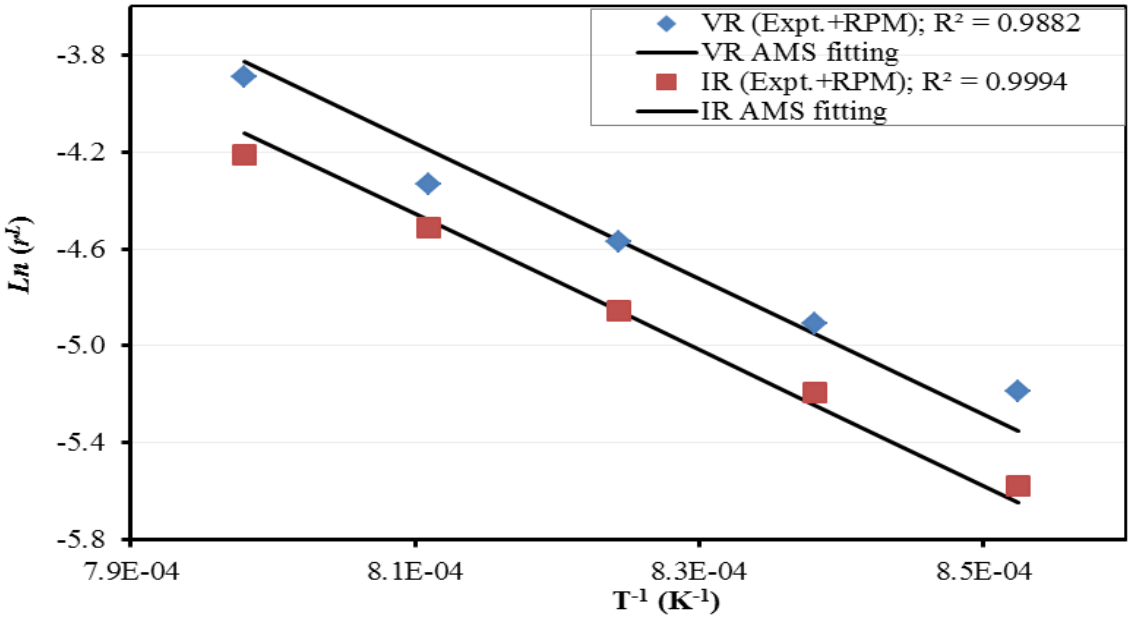

Fig 13. Validation of actvation energy calculated according to atomistic reaction kinetics with experimental results obtained from themogravimetric experimentation.

The results obtained from Equation (12) with respect to the lumped reaction rate (experimentally calculated and RPM evaluated) and the activation energy are also in good agreement with the results obtained from the atomistic modelling as shown in Figure 14. The pre-exponential factor was calculated from Equation (12) for CO_2 gas pressure of 875 kPa and using and order of reaction, n of 0.6 [6, 101]. The reaction kinetic parameters for the calculations are shown in Table 9. A comparison between the activation energy obtained from the respective procedures is presented in Figure 15.

Table 9. Estimated reaction parameters.

	Regressed Results		Atomistic modelling results (Activation energy validation)	
	IR	VR	IR	VR
E_a (kJ/mol)	210 ± 8	191 ± 25	233	233
k'_{S_0}	1.3E+05	9.7E+04	8.4E+07	1.1E+08

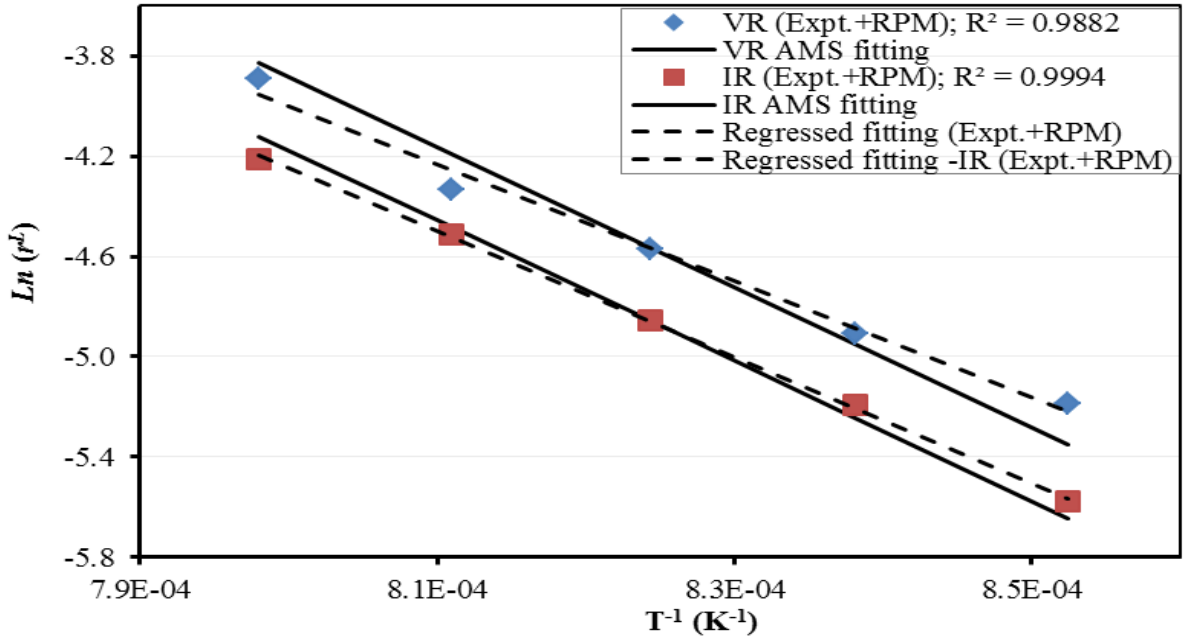

Fig 14. Comparison of experimental and model predictions.

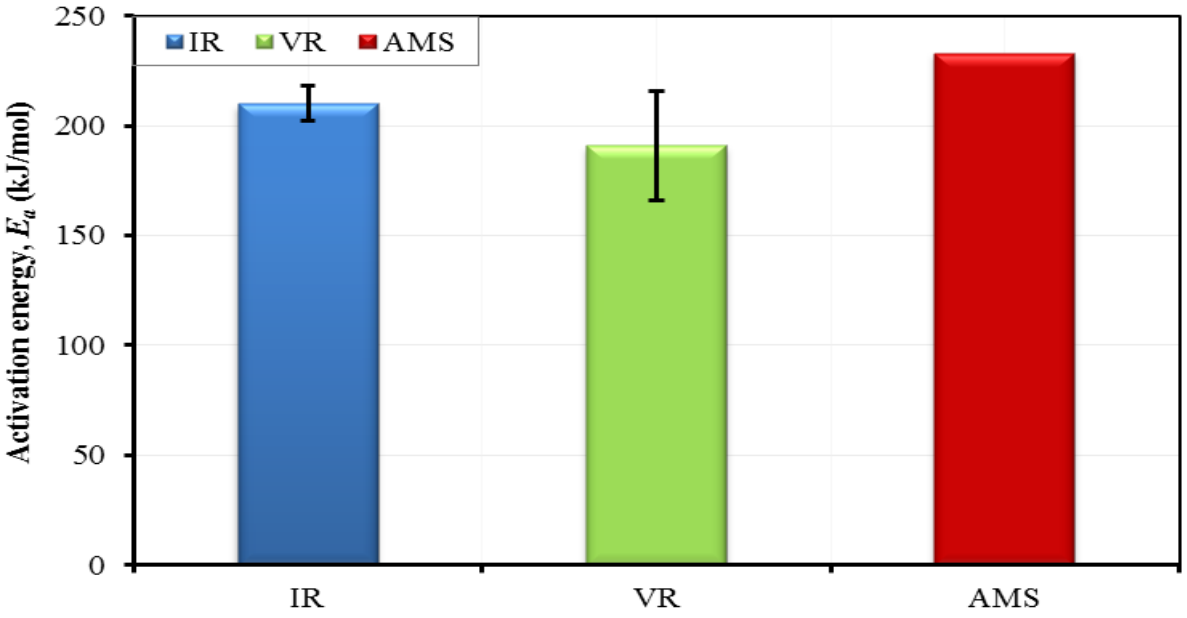

Fig 15. Comparison of activation energies.

4.2 Mechanisms of char gasification by CO_2

The CO_2 gasification occurs in regime I, which is chemically controlled. The salient features are the formation and accessibility of active sites, which in turn depends mostly on the

surface area formed during pyrolysis and formation of each char. The ΔE_b value for loss of H from C-H edges to form C* actives sites was calculated at a mean value of 472.5 kJ mol^{-1}. This value is higher than the computed mean barrier ΔE_b for dissociation of CO_2 to yield the first CO molecule (424.9 kJ mol^{-1}) for all active sites comprising the reactive edge. It is also higher than the mean value for loss of the second CO, ΔE_b of 233 kJ mol^{-1}. The experimental values E_a, was 191 ± 25 kJ mol^{-1} and 210 ± 8 kJ mol^{-1} for the de-ashed vitrinite- and inertinite-rich chars, respectively. The experimental results are in agreement with the computed values, and support mechanism that commences with the presence of actives sites on the char, formed during pyrolysis and char formation. If we assume that active sites may form purely through thermal decomposition of edge C-H groups to yield C* active sties, the major step in the mechanism of CO_2 gasification would be the formation of actives sites in char (and a larger value of experimentally determined activation energy). The experimental value also may indicate the likely sites for the thermal decomposition of CO_2 to yield the first CO at sites Czi and Cz (Table 6). The difficulties associated with a small graphene molecule to model coal char however, are amply demonstrated in the present work. The data supports a mechanism for CO_2 gasification of coal-char begins when active sites are liberated as the coal is heated to high temperatures. Therefore, the following descriptive mechanism is proposed and presented in Figure 16:

A. Chemisorption of CO_2 to active sites in char: The various C* sites located at a reactive edge may be classified as weak and strong. (This should not be confused with the strong and weak adsorption sites for CO_2 reported by Xu et al [109], related to the presence of inorganics in char). Strong adsorption is related to the formation of five member rings between two adjacent C* sites and adsorbed CO_2, whereas weakly adsorbed CO_2 occurs at a single C* site.

B. Yield of the first CO molecule: Two structures may form; one is a stable chemisorbed CO_2 molecule which encounters a lower energy barrier to dissociation, and the other a linear CO_2 molecule adsorbed on a single C* sites, which encounters a higher energy barrier to dissociation.

C. Yield of the second CO: A number of quinone-type char(CO) structures form after loss of the first CO. Those structures may decompose to form CO and relatively stable

five member carbon rings in char; however where stable five-membered rings are not energetically favoured, these do not undergo ring formation but instead form additional C* active sites for further gasification with CO_2. This decomposition reaction is defined as gasification `because of its distinction as rate limiting [119, 126].

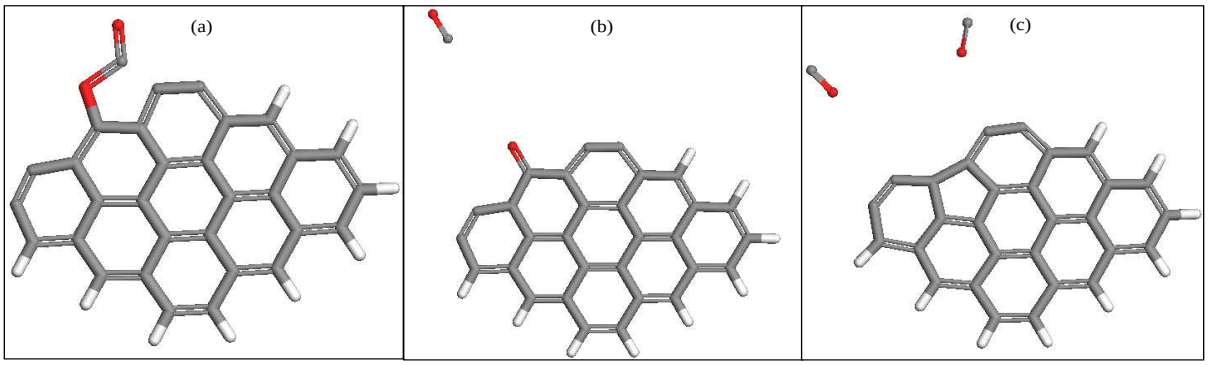

Fig 16. Mechanisms of char gasification by CO_2, where (a) = chemisorption of CO_2 to active sites in char, (b) = yield of first CO and (c) = yield of second CO.

5. Conclusions

The DFT modelling of CO_2 char gasification for the de-ashed vitrinite- and inertinite-rich chars provides details of the nature of reactive sites in chars structures, and also demonstrates the limitations inherent in using small molecular models in these studies. A combination of computer modelling and experimental techniques however, elucidated the diverse nature of active sites in these structures, the various mechanisms for chemisorption of CO_2 on active sites, dissociation of CO_2 into CO and O-complex; the loss of O-complex as CO and resulting char structures. The Fukui function $f^+(r)$ was a useful indicator of the preferred site for chemisorption of CO_2. The mean reactivity of H-saturated edge carbons decreased with increasing char molecules and was distributed according to the sequence: zigzag > armchair > tip active sites. In particular, the reactivity of the zigzag active sites decreased with increasing distances from the tip carbons. The average computed energy barrier of 233 kJ mol^{-1} compares well with the experimentally measured activation energy of 191 ± 25 kJ mol^{-1} and 210 ± 8 kJ mol^{-1} for the de-ashed vitrinite- and inertinite-rich chars, respectively. Consequently, the results show a reasonable agreement between DFT modelling outcomes and experimental results. Further work is required using a larger molecular model (provided

sufficient computer resources are available) to provide additional insights on the mechanisms of coal-char gasification.

6. Acknowledgements

This work is based on the research supported by the South African Research Chairs Initiative of the Department of Science and Technology and National Research Foundation (NRF) of South Africa (Chair Grant No. 86880, UID85643, Grant No. 85632). Any opinion, finding or conclusion or recommendation expressed in this material is that of the author(s) and the NRF does not accept any liability in this regard. The authors also wish to acknowledge the South African National Energy Development Institute (SANEDI) for initial financial support and the National Centre for High Performance Computing, Cape Town, South Africa.

References

1. Everson, R. C., Neomagus, H. W. J. P., Kaitano, R., Falcon, R., Alphen, C. v., du Cann, V. M., Properties of high ash char particles derived from inertinite-rich coal: 1. Chemical, structural and petrographic characteristics. Fuel, 2008. **87**(13-14): p. 3082-3090.
2. Everson, R. C., Neomagus, H. W. J. P., Kasaini, H., Njapha, D., Reaction kinetics of pulverized coal chars derived from inertinite-rich coal discards: Gasification with carbon dioxide and steam. Fuel, 2006. **85**(7–8): p. 1076-1082.
3. Chen, N., Yang, R. T., Ab initio molecular orbital calculation on graphite: Selection of molecular system and model chemistry. Carbon, 1998. **36**(7-8): p. 1061-1070.
4. Collot, A.-G., Matching gasification technologies to coal properties. International Journal of Coal Geology, 2006. **65**(3): p. 191-212.
5. Cousins, A., Paterson, N., Dugwell, D. R., Kandiyoti, R., An investigation of the reactivity *of chars formed in fluidized bed gasifiers: The effect of reaction conditions and particle size* on coal char reactivity. Energy & Fuels, 2006. **20**(6): p. 2489-2497.
6. Everson, R. C., Okolo, G. N., Neomagus, H. W. J. P., dos Santos, J.-M., X-ray diffraction parameters and reaction rate modeling for gasification and combustion of chars derived from inertinite-rich coals. Fuel, 2013. **109**(0): p. 148-156.
7. Hattingh, B. B., Everson, R. C., Neomagus, H. W., Bunt, J. R., Assessing the catalytic effect of coal ash constituents on the CO2 gasification rate of high ash, South African coal. Fuel Processing Technology, 2011. **92**(10): p. 2048-2054.
8. Golovina, E., Klimov, A., On the true kinetic constant of the heterogeneous C+ CO2 gasification reaction. Combustion, Explosion, and Shock Waves, 1999. **35**(4): p. 393-396.
9. Irfan, M. F., Usman, M. R., Kusakabe, K., Coal gasification in CO2 atmosphere and its kinetics since 1948: A brief review. Energy, 2011. **36**(1): p. 12-40.
10. Kajitani, S., Hara, S., Matsuda, H., Gasification rate analysis of coal char with a pressurized drop tube furnace. Fuel, 2002. **81**(5): p. 539-546.
11. Kajitani, S., Suzuki, N., Ashizawa, M., Hara, S., CO2 gasification rate analysis of coal char in entrained flow coal gasifier. Fuel, 2006. **85**(2): p. 163-169.
12. Kajitani, S., Tay, H.-L., Zhang, S., Li, C.-Z., Mechanisms and kinetic modelling of steam gasification of brown coal in the presence of volatile–char interactions. Fuel, 2013. **103**: p. 7-13.
13. Umemoto, S., Kajitani, S., Hara, S., Modeling of coal char gasification in coexistence of CO2 and H2O considering sharing of active sites. Fuel, 2013. **103**(0): p. 14-21.
14. Zhang, Y., Hara, S., Kajitani, S., Ashizawa, M., Modeling of catalytic gasification kinetics of coal char and carbon. Fuel, 2010. **89**(1): p. 152-157.
15. Bhatia, S. K., Reactivity of chars and carbons: New insights through molecular modeling. AIChE Journal, 1998. **44**(11): p. 2478-2493.
16. Gale, T. K., Bartholomew, C. H., Fletcher, T. H., Effects of pyrolysis heating rate on intrinsic reactivities of coal chars. Energy & Fuels, 1996. **10**(3): p. 766-775.
17. Johnson, C. A., Patrick, J. W., Mark Thomas, K., Characterization of coal chars by Raman spectroscopy, X-ray diffraction and reflectance measurements. Fuel, 1986. **65**(9): p. 1284-1290.
18. Matsui, I., Kojima, T., Kunii, D., Furusawa, T., Study of char gasification by carbon dioxide. 2. Continuous gasification in fluidized bed. Industrial & Engineering Chemistry Research, 1987. **26**(1): p. 95-100.
19. Wu, S., Gu, J., Zhang, X., Wu, Y., Gao, J., Variation of carbon crystalline structures and CO2 gasification reactivity of Shenfu coal chars at elevated temperatures. Energy & Fuels, 2007. **22**(1): p. 199-206.
20. Chen, S. G., Yang, R. T., Kapteijn, F., Moulijn, J. A., A new surface oxygen complex on carbon: toward a unified mechanism for carbon gasification reactions. Industrial & Engineering Chemistry Research, 1993. **32**(11): p. 2835-2840.
21. Frankcombe, T. J., Smith, S. C., On the microscopic mechanism of carbon gasification: A theoretical study. Carbon, 2004. **42**(14): p. 2921-2928.

22. Chen, J. P., Yang, R. T., Chemisorption of hydrogen on different planes of graphite — A semi-empirical molecular orbital calculation. Surface Science, 1989. **216**(3): p. 481-488.
23. Chen, S., Yang, R., Unified mechanism of alkali and alkaline earth catalyzed gasification reactions of carbon by CO2 and H2O. Energy & fuels, 1997. **11**(2): p. 421-427.
24. Espinal, J. F., Montoya, A., Mondragón, F., Truong, T. N., A DFT study of interaction of carbon monoxide with carbonaceous materials. The Journal of Physical Chemistry B, 2003. **108**(3): p. 1003-1008.
25. García, P., Espinal, J. F., Salinas Martínez de Lecea, C., Mondragón, F., Experimental characterization and molecular simulation of nitrogen complexes formed upon NO-char reaction at 270 °C in the presence of H2O and O2. Carbon, 2004. **42**(8-9): p. 1507-1515.
26. Espinal, J. F., Mondragón, F., Truong, T. N., Thermodynamic evaluation of steam gasification mechanisms of carbonaceous materials. Carbon, 2009. **47**(13): p. 3010-3018.
27. Frankcombe, T. J., Bhatia, S. K., Smith, S. C., Ab initio modelling of basal plane oxidation of graphenes and implications for modelling char combustion. Carbon, 2002. **40**(13): p. 2341-2349.
28. Radovic, L. R., The mechanism of CO2 chemisorption on zigzag carbon active sites: A computational chemistry study. Carbon, 2005. **43**(5): p. 907-915.
29. Radovic, L. R., Steczko, K., Walker Jr, P. L., Jenkins, R. G., Combined effects of inorganic constituents and pyrolysis conditions on the gasification reactivity of coal chars. Fuel Processing Technology, 1985. **10**(3): p. 311-326.
30. Radović, L. R., Walker Jr, P. L., Jenkins, R. G., Importance of carbon active sites in the gasification of coal chars. Fuel, 1983. **62**(7): p. 849-856.
31. Walker Jr, P., Rusinko Jr, F., Austin, L., Eley, D., Selwood, P., Weisz, P., Advances in Catalysis, vol. Vol. II, 1959: p. 133.
32. Walker Jr, P., Taylor, R., Ranish, J., An update on the carbon-oxygen reaction. Carbon, 1991. **29**(3): p. 411-421.
33. Domazetis, G., James, B., Liesegang, J., Computer molecular models of low-rank coal and char containing inorganic complexes. Journal of Molecular Modeling, 2008. **14**(7): p. 581-597.
34. Domazetis, G., Raoarun, M., James, B. D., Semiempirical and density functional theory molecular modeling of brown coal chars with iron species and H2, CO Formation. Energy & Fuels, 2007. **21**(5): p. 2531-2542.
35. Domazetis, G., Raoarun, M., James, B. D., Liesegang, J., Molecular modelling and experimental studies on steam gasification of low-rank coals catalysed by iron species. Applied Catalysis A: General, 2008. **340**(1): p. 105-118.
36. Samaras, P., Diamadopoulos, E., Sakellaropoulos, G. P., The effect of mineral matter and pyrolysis conditions on the gasification of Greek lignite by carbon dioxide. Fuel, 1996. **75**(9): p. 1108-1114.
37. Petersen, T., Yarovsky, I., Snook, I., McCulloch, D. G., Opletal, G., Microstructure of an industrial char by diffraction techniques and Reverse Monte Carlo modelling. Carbon, 2004. **42**(12): p. 2457-2469.
38. Montoya, A., Mondragón, F., Truong, T. N., First-principles kinetics of CO desorption from oxygen species on carbonaceous surface. The Journal of Physical Chemistry A, 2002. **106**(16): p. 4236-4239.
39. Montoya, A., Mondragón, F., Truong, T. N., CO2 adsorption on carbonaceous surfaces: a combined experimental and theoretical study. Carbon, 2003. **41**(1): p. 29-39.
40. Sendt, K., Haynes, B. S., Density functional study of the chemisorption of O2 on the armchair surface of graphite. Proceedings of the Combustion Institute, 2005. **30**(2): p. 2141-2149.
41. Sendt, K., Haynes, B. S., Density functional study of the reaction of O2 with a single site on the zigzag edge of graphene. Proceedings of the Combustion Institute, 2011. **33**(2): p. 1851-1858.
42. Sendt, K., Haynes, B. S., Density functional study of the chemisorption of O2 on the zig-zag surface of graphite. Combustion and Flame, 2005. **143**(4): p. 629-643.

43. Radovic, L. R., Active sites in graphene and the mechanism of CO2 formation in carbon oxidation. Journal of the American Chemical Society, 2009. **131**(47): p. 17166-17175.
44. Radovic, L. R., Jiang, H., Lizzio, A. A., A transient kinetics study of char gasification in carbon dioxide and oxygen. Energy & fuels, 1991. **5**(1): p. 68-74.
45. Roberts, M. J., Everson, R. C., Neomagus, H. W. J. P., Van Niekerk, D., Mathews, J. P., Branken, D. J., Influence of maceral composition on the structure, properties and behaviour of chars derived from South African coals. Fuel, 2015. **142**(0): p. 9-20.
46. Ahuja, P., Kumar, S., Singh, P. C., A model for primary and heterogeneous secondary reactions of wood pyrolysis. Chemical engineering & technology, 1996. **19**(3): p. 272-282.
47. Xu, W.-C., Tomita, A., Effect of coal type on the flash pyrolysis of various coals. Fuel, 1987. **66**(5): p. 627-631.
48. Dyrkacz, G. R., Bloomquist, C. A. A., Use of continuous flow centrifugation techniques for coal maceral separation. 2. Multiple density fractionations of coals. Energy & Fuels, 1992. **6**(4): p. 374-386.
49. Bolat, E., Saglam, S., Piskin, S., Chemical demineralization of a Turkish high ash bituminous coal. Fuel Processing Technology, 1998. **57**(2): p. 93-99.
50. Joseph, J. T., Fisher, R. B., Masin, C. A., Dyrkacz, G. R., Bloomquist, C. A., Winans, R. E., Coal maceral chemistry. 1. Liquefaction behavior. Energy & Fuels, 1991. **5**(5): p. 724-729.
51. Van Niekerk, D., Pugmire, R. J., Solum, M. S., Painter, P. C., Mathews, J. P., Structural characterization of vitrinite-rich and inertinite-rich Permian-aged South African bituminous coals. International Journal of Coal Geology, 2008. **76**(4): p. 290-300.
52. Wijaya, N., Zhang, L., A Critical review of coal demineralization and its implication on understanding the speciation of organically bound metals and submicrometer mineral grains in coal. Energy & Fuels, 2011. **25**(1): p. 1-16.
53. Mathews, J. P., Fernandez-Also, V., Daniel Jones, A., Schobert, H. H., Determining the molecular weight distribution of Pocahontas No. 3 low-volatile bituminous coal utilizing HRTEM and laser desorption ionization mass spectra data. Fuel, 2010. **89**(7): p. 1461-1469.
54. Niekerk, D. V., Mathews, J. P., Molecular representations of Permian-aged vitrinite-rich and inertinite-rich South African coals. Fuel, 2010. **89**(1): p. 73-82.
55. Sharma, A., Kyotani, T., Tomita, A., A new quantitative approach for microstructural analysis of coal char using HRTEM images. Fuel, 1999. **78**(10): p. 1203-1212.
56. Panik, M. J., Advanced statistics from an elementary point of view. Vol. 9. 2005: Academic Press.
57. Fernandez-Alos, V., Watson, J. K., Wal, R. v., Mathews, J. P., Soot and char molecular representations generated directly from HRTEM lattice fringe images using Fringe3D. Combustion and Flame, 2011. **158**(9): p. 1807-1813.
58. Castro-Marcano, F., Kamat, A. M., Russo Jr, M. F., van Duin, A. C. T., Mathews, J. P., Combustion of an Illinois No. 6 coal char simulated using an atomistic char representation and the ReaxFF reactive forcefield. Combustion and Flame, 2012. **159**(3): p. 1272-1285.
59. Pham, B. Q., Truong, T. N., Electronic spin transitions in finite-size graphene. Chemical Physics Letters, 2012. **535**(0): p. 75-79.
60. Radovic, L. R., Bockrath, B., On the c*hemical nature of graphene edges: Origin of stability* and potential for magnetism in carbon materials. Journal of the American Chemical Society, 2005. **127**(16): p. 5917-5927.
61. Marinov, N., Pitz, W., Westbrook, C., Castaldi, M., Senkan, S., Modeling of aromatic and polycyclic aromatic hydrocarbon formation in premixed methane and ethane flames. Combustion Science and Technology, 1996. **116**(1-6): p. 211-287.
62. Kunioshi, N. l., Touda, M., Fukutani, S., Computational study on the formation of five-membered rings in pah through reaction with O2. Combustion and flame, 2002. **128**(3): p. 292-300.
63. Montoya, A., Truong, T.-T. T., Mondragón, F., Truong, T. N., CO desorption from oxygen *species on carbonaceous surface: 1. Effects of the local structure o*f the active site and the surface coverage. The Journal of Physical Chemistry A, 2001. **105**(27): p. 6757-6764.

64. Montoya, A., Mondragón, F., Truong, T. N., Adsorption on carbonaceous surfaces: cost-effective computational strategies for quantum chemistry studies of aromatic systems. Carbon, 2002. **40**(11): p. 1863-1872.
65. Solum, M. S., Sarofim, A. F., Pugmire, R. J., Fletcher, T. H., Zhang, H., 13C NMR analysis of soot produced from model compounds and a coal. Energy & Fuels, 2001. **15**(4): p. 961-971.
66. Solum, M. S., Pugmire, R. J., Grant, D. M., Carbon-13 solid-state NMR of Argonne-premium coals. Energy & Fuels, 1989. **3**(2): p. 187-193.
67. Perry, S., Hambly, E., Fletcher, T., Solum, M., Pugmire, R., Solid-state carbon-13 NMR characterization of matched tars and chars from rapid coal devolatilization. Proceedings of the Combustion Institute, 2000. **28**(2): p. 2313-2319.
68. Perry, S. T., Hambly, E. M., Fletcher, T. H., Solum, M. S., Pugmire, R. J., Solid-state 13C NMR characterization of matched tars and chars from rapid coal devolatilization. Proceedings of the Combustion Institute, 2000. **28**(2): p. 2313-2319.
69. Delley, B., From molecules to solids with the DMol3 approach. The Journal of Chemical Physics, 2000. **113**(18): p. 7756-7764.
70. Perdew, J. P., Wang, Y., Accurate and simple analytic representation of the electron-gas correlation energy. Physical Review B, 1992. **45**(23): p. 13244-13249.
71. Furche, F., Perdew, J. P., The performance of semilocal and hybrid density functionals in 3d transition-metal chemistry. The Journal of Chemical Physics, 2006. **124**(4): p. 044103-27.
72. Henkelman, G., Jóhannesson, G., Jónsson, H., Methods for finding saddle points and minimum energy paths, in Theoretical Methods in Condensed Phase Chemistry, S. Schwartz, Editor. 2002, Springer Netherlands. p. 269-302.
73. Henkelman, G., Uberuaga, B. P., Jónsson, H., A climbing image nudged elastic band method for finding saddle points and minimum energy paths. The Journal of Chemical Physics, 2000. **113**(22): p. 9901-9904.
74. Sheppard, D., Terrell, R., Henkelman, G., Optimization methods for finding minimum energy paths. The Journal of Chemical Physics, 2008. **128**(13): p. -.
75. Jónsson, H., Mills, G., Jacobsen, K. W., Nudged elastic band method for finding minimum energy paths of transition, in Classical and quantum dynamics in condensed phase simulations. 1998, World Scientific. p. 385-404.
76. Roy, R. K., Pal, S., Hirao, K., On non-negativity of Fukui function indices. The Journal of chemical physics, 1999. **110**(17): p. 8236-8245.
77. Kusama, H., Orita, H., Sugihara, H., DFT investigation of the TiO2 band shift by nitrogen-containing heterocycle adsorption and implications on dye-sensitized solar cell performance. Solar Energy Materials and Solar Cells, 2008. **92**(1): p. 84-87.
78. Pulay, P., Improved SCF convergence acceleration. Journal of Computational Chemistry, 1982. **3**(4): p. 556-560.
79. Sablon, N., Proft, F. D., Geerlings, P., Molecular orbital-averaged Fukui function for the reactivity description of alkaline earth metal oxide clusters. Journal of Chemical Theory and Computation, 2009. **5**(5): p. 1245-1253.
80. Bultinck, P., Fias, S., Van Alsenoy, C., Ayers, P., Carbó-Dorca, R., Critical thoughts on computing atom condensed Fukui functions. The Journal of Chemical Physics, 2007. **127**(3): p. 034102.
81. Fukui, K., Theory of orientation and stereoselection, in Orientation and Stereoselection. 1970, Springer Berlin Heidelberg. p. 1-85.
82. Fuentealba, P., Pérez, P., Contreras, R., On the condensed Fukui function. The Journal of Chemical Physics, 2000. **113**(7): p. 2544-2551.
83. Chattaraj, P. K., *Chemical reactivity and selectivity: Local HSAB principle versus frontier* orbital theory. The Journal of Physical Chemistry A, 2000. **105**(2): p. 511-513.
84. Melin, J., Aparicio, F., Subramanian, V., Galván, M., Chattaraj, P. K., Is the Fukui function *a right descriptor of hard−hard interactions?* The Journal of Physical Chemistry A, 2004. **108**(13): p. 2487-2491.
85. Parr, R. G., Yang, W., Density functional approach to the frontier-electron theory of chemical reactivity. Journal of the American Chemical Society, 1984. **106**(14): p. 4049-4050.

86. Pérez, P., Simón-Manso, Y., Aizman, A., Fuentealba, P., Contreras, R., Empirical *energy−density relationships f*or the analysis of substituent effects in chemical reactivity. Journal of the American Chemical Society, 2000. **122**(19): p. 4756-4762.
87. Li, Y., Evans, J. N. S., The Fukui function: A key concept linking frontier molecular orbital theory and the hard-soft-acid-base principle. Journal of the American Chemical Society, 1995. **117**(29): p. 7756-7759.
88. Fusaro, M., Barone, V., Causa, M., D'Amore, M., Garzillo, C., Theoretical analysis of the reactivity of carbon nanotubes: local versus topological effects, in Topological Modelling of Nanostructures and Extended Systems. 2013, Springer. p. 303-323.
89. Ergun, S., Yasinsky, J. B., Townsend, J. R., Transverse and longitudinal optical properties of graphite. Carbon, 1967. **5**(4): p. 403-408.
90. Montoya, A., Mondragón, F., Truong, T. N., Formation of CO precursors during char gasification with O2, CO2 and H2O. Fuel Processing Technology, 2002. **77-78**: p. 125-130.
91. Moulijn, J. A., Kapteijn, F., Towards a unified theory of reactions of carbon with oxygen-containing molecules. Carbon, 1995. **33**(8): p. 1155-1165.
92. Chen, S. G., Yang, R. T., Unified mechanism of alkali and alkaline earth catalyzed gasification reactions of carbon by CO2 and H2O. Energy & Fuels, 1997. **11**(2): p. 421-427.
93. Hunt, J., Ferrari, A., Lita, A., Crosswhite, M., Ashley, B., Stiegman, A. E., Microwave-specific enhancement of the carbon–carbon dioxide (Boudouard) reaction. The Journal of Physical Chemistry C, 2013. **117**(51): p. 26871-26880.
94. Govind, N., Petersen, M., Fitzgerald, G., King-Smith, D., Andzelm, J., A generalized synchronous transit method for transition state location. Computational materials science, 2003. **28**(2): p. 250-258.
95. Andzelm, J., Govind, N., Maiti, A., Nanotube-based gas sensors–Role of structural defects. Chemical Physics Letters, 2006. **421**(1): p. 58-62.
96. Andersen, A., Govind, N., Subramanian, L., Theoretical study of the mechanism behind the para-selective nitration of toluene in zeolite H-Beta. Molecular Simulation, 2008. **34**(10-15): p. 1025-1039.
97. Wigner, E., The transition state method. Trans. Faraday Soc., 1938. **34**: p. 29-41.
98. McLafferty, F. J., Pechukas, P., Quantum transition state theory. Chemical Physics Letters, 1974. **27**(4): p. 511-514.
99. Pechukas, P., Miller, W., Dynamics of molecular collisions. Part, 1976. **2**: p. 269.
100. Wang, S.-G., Cao, D.-B., Li, Y.-W., Wang, J., Jiao, H., CO2 reforming of CH4 on *Ni(111): A density functional theory calculation.* The Journal of Physical Chemistry B, 2006. **110**(20): p. 9976-9983.
101. Everson, R. C., Neomagus, H. W., Kaitano, R., Falcon, R., du Cann, V. M., Properties of high ash coal-char particles derived from inertinite-rich coal: II. Gasification kinetics with carbon dioxide. Fuel, 2008. **87**(15): p. 3403-3408.
102. Bhatia, S., Perlmutter, D., A random pore model for fluid-solid reactions: I. Isothermal, kinetic control. AIChE Journal, 1980. **26**(3): p. 379-386.
103. Raj, A., Zainuddin, Z., Sander, M., Kraft, M., A mechanistic study on the simultaneous elimination of soot and nitric oxide from engine exhaust. Carbon, 2011. **49**(5): p. 1516-1531.
104. Sander, M., Raj, A., Inderwildi, O., Kraft, M., Kureti, S., Bockhorn, H., The simultaneous reduction of nitric oxide and soot in emissions from diesel engines. Carbon, 2009. **47**(3): p. 866-875.
105. Montoya, A., Truong, T. N., Sarofim, A. F., Application of density functional theory to the study of the reaction of NO with char-bound nitrogen during combustion. The Journal of Physical Chemistry A, 2000. **104**(36): p. 8409-8417.
106. Zhang, S.-Y., Lu, J.-F., Zhang, J.-S., Yue, G.-X., Effect of pyrolysis intensity on the reactivity of coal char. Energy & Fuels, 2008. **22**(5): p. 3213-3221.
107. Senneca, O., Russo, P., Salatino, P., Masi, S., The relevance of thermal annealing to the evolution of coal char gasification reactivity. Carbon, 1997. **35**(1): p. 141-151.
108. Jones, J. M., Jones, D. H., Modelling the competition between annealing and oxidation in the carbon-oxygen reaction. Carbon, 2007. **45**(3): p. 677-680.

109. Xu, K., Hu, S., Su, S., Xu, C., Sun, L., Shuai, C., et al Xiang, J., Study on char surface active sites and their relationship to gasification reactivity. Energy & Fuels, 2012. **27**(1): p. 118-125.
110. Suuberg, E. M., Thermally induced changes in reactivity of carbons, in Fundamental issues in control of carbon gasification reactivity, J. Lahaye and P. Ehrburger, Editors. 1991, Springer Netherlands. p. 269-305.
111. Kyotani, T., Tomita, A., Analysis of the reaction of carbon with NO/N2O using ab initio molecular orbital theory. The Journal of Physical Chemistry B, 1999. **103**(17): p. 3434-3441.
112. Denisov, E. T., Denisova, T., Handbook of antioxidants: bond dissociation energies, rate constants, activation energies, and enthalpies of reactions. Vol. 100. 1999: CRC press.
113. Michaelides, A., Liu, Z.-P., Zhang, C., Alavi, A., King, D. A., Hu, P., Identification of general linear relationships between activation energies and enthalpy changes for dissociation reactions at surfaces. Journal of the American Chemical Society, 2003. **125**(13): p. 3704-3705.
114. Chandra, A. K., Uchimaru, T., A DFT study on the CH bond dissociation enthalpies of haloalkanes: Correlation between the bond dissociation enthalpies and activation energies for hydrogen abstraction. The Journal of Physical Chemistry A, 2000. **104**(40): p. 9244-9249.
115. Wu, X., Radovic, L. R., Ab initio molecular orbital study on the electronic structures and reactivity of Boron-substituted carbon. The Journal of Physical Chemistry A, 2004. **108**(42): p. 9180-9187.
116. Radovic, L. R., Bockrath, B., What exactly is on the edges of graphene layers in carbon: the unfolding story. Preprints Paper-American Chemical Society, Division of Fuel Chemistry, 2002. **47**(2): p. 428-431.
117. Radovic, L. R., Bockrath, B. On some key questions in the application of computational chemistry to carbon reactivity. in Proc. Conf. Carbon. 2001.
118. Kyotani, T., Ito, K. i., Tomita, A., Radovic, L. R., Monte Carlo simulation of carbon gasification using molecular orbital theory. AIChE journal, 1996. **42**(8): p. 2303-2307.
119. Zhu, Z. H., Finnerty, J., Lu, G. Q., Yang, R. T., A comparative study of carbon gasification with O2 and CO2 by density functional theory calculations. Energy & Fuels, 2002. **16**(6): p. 1359-1368.
120. Accelrys, E. c. w., Material Studio DMol^3 V6.0. Density Functional Theory Electronic Structure Program. Support Division. 2011.
121. Cao, D.-B., Li, Y.-W., Wang, J., Jiao, H., CO2 dissociation on Ni(2 1 1). Surface Science, 2009. **603**(19): p. 2991-2998.
122. Myers, A. L., Thermodynamics of adsorption in porous materials. AIChE Journal, 2002. **48**(1): p. 145-160.
123. Liu, Z.-S., Wang, Q., Zou, Z.-S., Tan, G.-L., Reaction mechanism of carbon gasification in CO2 under non-isothermal conditions. Journal of Thermal Analysis and Calorimetry, 2010: p. 1-6.
124. Cabrera-Sanfelix, P., Adsorption and reactivity of CO2 on defective graphene sheets. The Journal of Physical Chemistry A, 2008. **113**(2): p. 493-498.
125. Stans, M. H., Bond Dissociation Energies in Simple Molecules.
126. Chen, N., Yang, R. T., Ab initio molecular orbital study of the unified mechanism and pathways for gas-carbon reactions. The Journal of Physical Chemistry A, 1998. **102**(31): p. 6348-6356.
127. Miura, K., Makino, M., Silveston, P. L., Correlation of gasification reactivities with char properties and pyrolysis conditions using low rank Canadian coals. Fuel, 1990. **69**(5): p. 580-589.